Model Study of ATP and ADP Buffering, Transport of Ca²⁺ and Mg²⁺, and Regulation of Ion Pumps in Ventricular Myocyte

Anushka Michailova*[†] and Andrew McCulloch[†]

*Department of Biophysics, Bulgarian Academy of Science, Sofia, Bulgaria, and [†]Department of Bioengineering, University of California, San Diego, California 92093-0412 USA

ABSTRACT   We extended the model of the ventricular myocyte by Winslow et al. (*Circ. Res.* 1999, 84:571–586) by incorporating equations for Ca²⁺ and Mg²⁺ buffering and transport by ATP and ADP and equations for MgATP regulation of ion transporters (Na⁺-K⁺ pump, sarcolemmal and sarcoplasmic Ca²⁺ pumps). The results indicate that, under normal conditions, Ca²⁺ binding by low-affinity ATP and diffusion of CaATP may affect the amplitude and time course of intracellular Ca²⁺ signals. The model also suggests that a fall in ATP/ADP ratio significantly reduces sarcoplasmic Ca²⁺ content, increases diastolic Ca²⁺, lowers systolic Ca²⁺, increases Ca²⁺ influx through L-type channels, and decreases the efficiency of the Na⁺/Ca²⁺ exchanger in extruding Ca²⁺ during periodic voltage-clamp stimulation. The analysis suggests that the most important reason for these changes during metabolic inhibition is the down-regulation of the sarcoplasmic Ca²⁺-ATPase pump by reduced diastolic MgATP levels. High Ca²⁺ concentrations developed near the membrane might have a greater influence on Mg²⁺, ATP, and ADP concentrations than that of the lower Ca²⁺ concentrations in the bulk myoplasm. The model predictions are in general agreement with experimental observations measured under normal and pathological conditions.

GLOSSARY

Abbreviations

ATP = adenosine triphosphate
ADP = adenosine diphosphate
SR = sarcoplasmic reticulum
JSR = junctional sarcoplasmic reticulum
NSR = network sarcoplasmic reticulum
RyR = ryanodine receptor

Volumes, areas, and capacity

V_{ss} = subspace volume
V_{myo} = myoplasmic volume
V_{JSR} = junctional SR volume
A_{cap} = capacitive membrane area
C_{sc} = specific membrane capacity
F = Faraday constant

Membrane currents

I_{Na} = Na⁺ current
I_{Kr} = rapid-activating delayed rectifier K⁺ current
I_{Ks} = slow-activating delayed rectifier K⁺ current
I_{to1} = transient outward K⁺ current
I_{K1} = time-independent K⁺ current
I_{Kp} = plateau K⁺ current
I_{NaCa} = Na⁺-Ca²⁺ exchanger current
I_{NaK}^* = modified Na⁺-K⁺ pump current
$I_{p(Ca)}^*$ = modified sarcolemmal Ca²⁺ pump current

$I_{Ca,b}$ = Ca²⁺ background current
$I_{Na,b}$ = Na⁺ background current
I_{Ca} = L-type Ca²⁺ current
$I_{Ca,K}$ = K⁺ current through L-type Ca²⁺ channel

Concentrations

$[Na]_0$ = extracellular Na⁺ concentration
$[K]_0$ = extracellular K⁺ concentration
$[Ca]_0$ = extracellular Ca²⁺ concentration
$[Na]_i$ = intracellular Na⁺ concentration
$[K]_i$ = intracellular K⁺ concentration
$[Ca]_{ss}$ = free subspace Ca²⁺ concentration
$[Ca]_i$ = free myoplasmic Ca²⁺ concentration
$[Ca]_{JSR}$ = JSR Ca²⁺ concentration
$[Ca]_{NSR}$ = NSR Ca²⁺ concentration
$[Mg]_{tot}$ = total Mg²⁺ concentration
$[Mg]_{ss}$ = free subspace Mg²⁺ concentration
$[Mg]_i$ = free myoplasmic Mg²⁺ concentration
$[ATP]_{tot}$ = total ATP concentration
$[ATP]_{ss}$ = free subspace ATP concentration
$[ATP]_i$ = free myoplasmic ATP concentration
$[CaATP]_{ss}$ = subspace concentration of Ca²⁺-bound ATP
$[CaATP]_i$ = myoplasmic concentration of Ca²⁺-bound ATP
$[MgATP]_{ss}$ = subspace concentration of Mg²⁺-bound ATP
$[MgATP]_i$ = myoplasmic concentration of Mg²⁺-bound ATP
$[ADP]_{tot}$ = total ADP concentration
$[ADP]_{ss}$ = free subspace ADP concentration
$[ADP]_i$ = free myoplasmic ADP concentration
$[CaADP]_{ss}$ = subspace concentration of Ca²⁺-bound ADP
$[CaADP]_i$ = myoplasmic concentration of Ca²⁺-bound ADP
$[MgADP]_{ss}$ = subspace concentration of Mg²⁺-bound ADP
$[MgADP]_i$ = myoplasmic concentration of Mg²⁺-bound ADP

Fluxes

J_{xfer} = Ca²⁺ flux from subspace to myoplasm
J_{rel} = RyR channel Ca²⁺ flux

J_{up}^* = modified Ca^{2+} uptake into NSR by SR Ca^{2+}-ATPase pump

J_{trpn} = buffering of Ca^{2+} by troponin C

J_{xfer}^{Mg} = Mg^{2+} flux from subspace to myoplasm

J_{xfer}^{CaATP} = CaATP flux from subspace to myoplasm

J_{xfer}^{MgATP} = MgATP flux from subspace to myoplasm

J_{xfer}^{CaADP} = CaADP flux from subspace to myoplasm

J_{xfer}^{MgADP} = MgADP flux from subspace to myoplasm

Time constants

τ_{xfer} = time constant for transfer of Ca^{2+} from subspace to myoplasm

τ_{xfer}^{Mg} = time constant for transfer of Mg^{2+} from subspace to myoplasm

τ_{xfer}^{CaATP} = time constant for transfer of CaATP from subspace to myoplasm

τ_{xfer}^{MgATP} = time constant for transfer of MgATP from subspace to myoplasm

τ_{xfer}^{CaADP} = time constant for transfer of CaADP from subspace to myoplasm

τ_{xfer}^{MgADP} = time constant for transfer of MgADP from subspace to myoplasm

Dissociation and rate constants

K_D^{CaATP} = Ca^{2+}-ATP dissociation constant

k_+^{CaATP} = Ca^{2+} on-rate constant for ATP

k_-^{CaATP} = Ca^{2+} off-rate constant for ATP

K_D^{MgATP} = Mg^{2+}-ATP dissociation constant

k_+^{MgATP} = Mg^{2+} on-rate constant for ATP

k_-^{MgATP} = Mg^{2+} off-rate constant for ATP

K_D^{CaADP} = Ca^{2+}-ADP dissociation constant

k_+^{CaADP} = Ca^{2+} on-rate constant for ADP

k_-^{CaADP} = Ca^{2+} off-rate constant for ADP

K_D^{MgADP} = Mg^{2+}-ADP dissociation constant

k_+^{MgADP} = Mg^{2+} on-rate constant for ADP

k_-^{MgADP} = Mg^{2+} off-rate constant for ADP

INTRODUCTION

A number of mathematical models have been developed to investigate Ca^{2+} signaling in cardiac muscle cells (Robertson et al., 1981; Michailova and Spassov, 1992; Stern, 1992; Amstudz et al., 1996; Keizer and Levine, 1996; Langer and Peskoff, 1996; Negroni and Lascano, 1996; Soeller and Cannell, 1997; Jafri et al., 1998; Hunter et al., 1998; Nygren et al., 1998; Peskoff and Langer, 1998; Winslow et al., 1998, 1999; Dawson et al., 1999; Michailova et al., 1999; Rice et al., 1999; Zoghbi et al., 2000). However, these models cannot be used to predict how the binding and transport of Ca^{2+} and Mg^{2+} by the mobile buffers, ATP and ADP, or a fall in [ATP]$_{tot}$/[ADP]$_{tot}$ ratio might modulate intracellular Ca^{2+}, Mg^{2+}, Na$^+$, and K$^+$ concentrations, ion pumps and currents, or, conversely, how changes in free

Ca^{2+} concentrations during excitation could alter free and bound concentrations of ATP and ADP. Recently, ATP diffusion and Ca^{2+} and Mg^{2+} exchange with ATP have been introduced in models of smooth muscle cells (Kargacin and Kargacin, 1997) and skeletal muscle cells (Baylor and Hollingworth, 1998). Cardiac energetics (metabolism of high-energy phosphates, glycogen metabolism, and lactate transport) and pH regulation have also been integrated with electrophysiological models (Ch'en et al., 1997, 1998; Shaw and Rudy, 1997).

Winslow et al. (1999) modified the model of Jafri et al. (1998) for guinea pig ventricular cells to study the mechanisms of Ca^{2+} handling in the canine midmyocardial ventricular myocytes. This integrative model incorporated: 1) membrane ion currents from the Luo–Rudy phase II ventricular cell model (Luo and Rudy, 1994); 2) the formulation of Jafri et al. (1998) for the L-type Ca^{2+} current that exhibits the mode-switching behavior observed by Imredy and Yue (1994); 3) SR Ca^{2+} release from RyR channels described in the Keizer and Levine (1996) model with receptor adaptation; 4) a subsarcolemmal space; 5) Ca^{2+} buffering by low- and high-affinity Ca^{2+} binding sites on troponin, and Ca^{2+} buffering by calmodulin and calsequestrin. In the model of Winslow et al. (1999), calculated subsarcolemmal Ca^{2+} could reach high levels (~30 μM) during excitation and rose more rapidly than myoplasmic Ca^{2+} (~0.5–0.6 μM). It faithfully reproduced measured Ca^{2+} transients in normal and failing canine ventricular myocytes (O'Rourke et al., 1999).

In this study, we extend the model of Winslow et al. (1999) by incorporating equations for Ca^{2+} and Mg^{2+} buffering and transport by ATP and ADP and equations describing ATP (or MgATP) regulation of ion transporters (Na$^+$-K$^+$ ATPase pump, sarcolemmal Ca^{2+}-ATPase pump, SR Ca^{2+}-ATPase pump). Our results support the hypothesis that, under normal conditions, Ca^{2+} binding by low-affinity mobile buffer ATP and diffusion of Ca^{2+}-bound ATP (CaATP) may contribute to the amplitude and time course of intracellular Ca^{2+} signals. The inclusion of ATP and ADP buffering slightly decreased the peak of the myoplasmic Ca^{2+} transient computed in response to periodic voltage-clamp stimuli. The addition of CaATP diffusion slightly decreased the peak and accelerated the relaxation of the Ca^{2+} transient in the subspace. Metabolic changes (a fall in [ATP]$_{tot}$/[ADP]$_{tot}$ ratio) significantly reduced SR Ca^{2+} content, increased diastolic Ca^{2+} levels, and decreased systolic Ca^{2+} levels computed in response to periodic voltage-clamp stimuli. As a result, Ca^{2+} influx through L-type Ca^{2+} channels increased while the efficiency of Ca^{2+} extrusion by the Na$^+$/Ca^{2+} exchanger decreased. The main reason for these changes was reduced Ca^{2+} uptake by the SR Ca^{2+}-ATPase (SERCA2a pump) due to decreased diastolic MgATP levels during metabolic inhibition. In ventricular myocytes, high Ca^{2+} concentrations developed near the membrane might influence Mg^{2+}, ATP, and ADP concen-
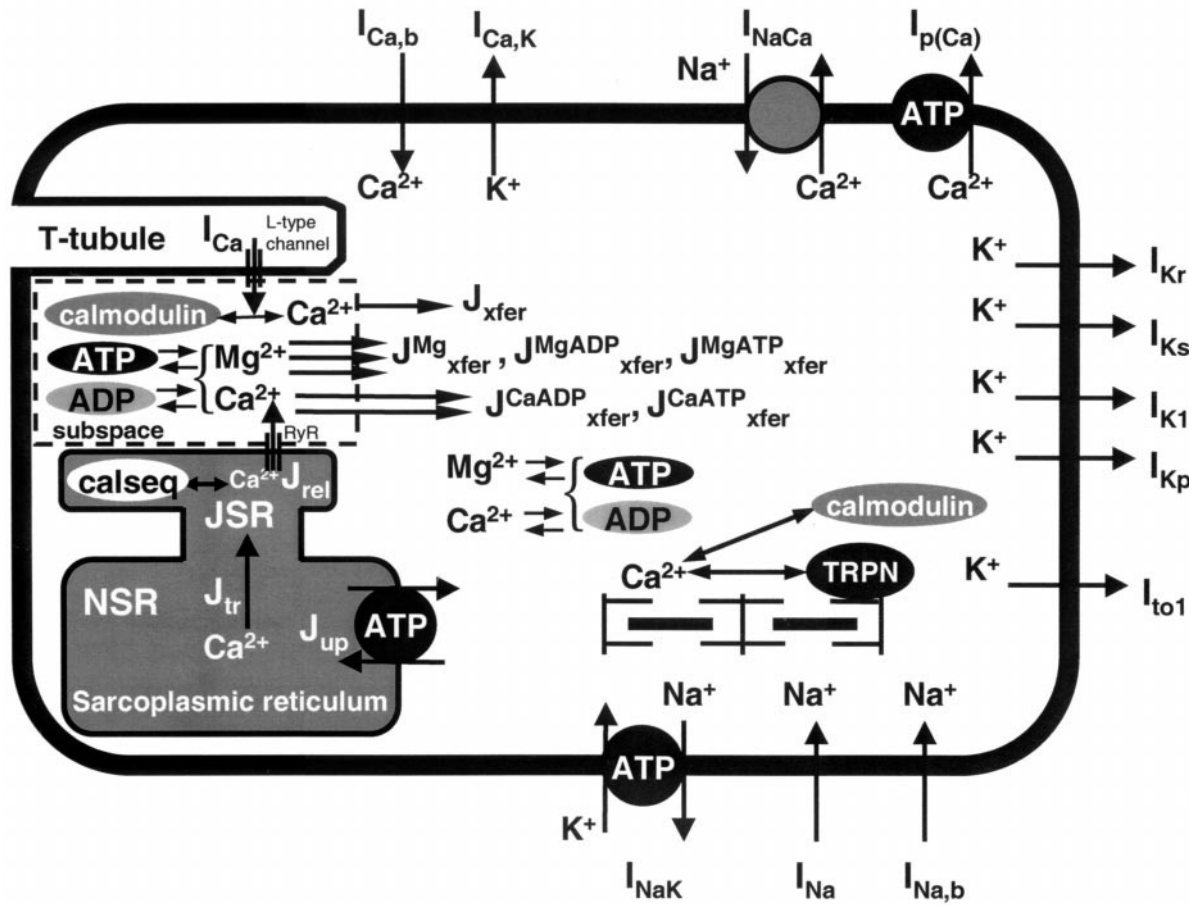
FIGURE 1 Schematic diagram of the mechanisms involved in the model.

trations more significantly than the negligible alterations in these concentrations stimulated by low myoplasmic Ca^{2+}.

MATHEMATICAL MODEL

The overall scheme of the model is shown in Fig. 1. (See Glossary for the notations of the parameters used throughout the study.) We provide only the additional or modified equations necessary to include ATP and ADP as Ca^{2+} and Mg^{2+} buffers and transporters, and ATP as Na^+-K^+, sarcolemmal, and SR Ca^{2+} pumps regulator. The remaining equations were the same as those in the original paper of Winslow et al. (1999) with the corrections as given on the author's web site.

Experimental data suggest that the SR is not accessible to the mobile buffers, ATP and ADP (Bers, 1991; Carmeliet, 1999). Therefore, in the model, ATP and ADP are free to react and diffuse within the subspace and bulk myoplasm but not in the SR (Fig. 1). It was also assumed that the total ATP and ADP concentrations in the subspace ($[ATP]_{tot-ss}$, $[ADP]_{tot-ss}$) and bulk myoplasm ($[ATP]_{tot-i}$, $[ADP]_{tot-i}$) are equal, spatially uniform, and remain constant during excitation, i.e.,

$$[ATP]_{tot} = [ATP]_{tot-i} = [ATP]_{tot-ss}, \tag{1}$$

$$[ADP]_{tot} = [ADP]_{tot-i} = [ADP]_{tot-ss} \tag{2}$$

The buffering of Ca^{2+} and Mg^{2+} by ATP in the subspace is given by the following equations:

$$[ATP]_{ss} = [ATP]_{tot} - [CaATP]_{ss} - [MgATP]_{ss}, \tag{3}$$

$$\frac{d[CaATP]_{ss}}{dt} = -J_{xfer}^{CaATP}\frac{V_{myo}}{V_{ss}} + k_+^{CaATP}[Ca]_{ss}[ATP]_{ss}$$
$$- k_-^{CaATP}[CaATP]_{ss}, \tag{4}$$

$$\frac{d[MgATP]_{ss}}{dt} = -J_{xfer}^{MgATP}\frac{V_{myo}}{V_{ss}} + k_+^{MgATP}[Mg]_{ss}[ATP]_{ss}$$
$$- k_-^{MgATP}[MgATP]_{ss}, \tag{5}$$

where k_+ and k_- are the corresponding on-rate and off-rate binding constants. The equations for the bulk myoplasm are similar:

$$[ATP]_i = [ATP]_{tot} - [CaATP]_i - [MgATP]_i, \tag{6}$$

$$\frac{d[\text{CaATP}]_i}{dt} = J_{\text{xfer}}^{\text{CaATP}} + k_+^{\text{CaATP}}[\text{Ca}]_i[\text{ATP}]_i$$
$$- k_-^{\text{CaATP}}[\text{CaATP}]_i, \qquad (7)$$

$$\frac{d[\text{MgATP}]_i}{dt} = J_{\text{xfer}}^{\text{MgATP}} + k_+^{\text{MgATP}}[\text{Mg}]_i[\text{ATP}]_i$$
$$- k_-^{\text{MgATP}}[\text{MgATP}]_i, \qquad (8)$$

CaATP and MgATP fluxes (Fig. 1) are given by

$$J_{\text{xfer}}^{\text{CaATP}} = \frac{[\text{CaATP}]_{\text{ss}} - [\text{CaATP}]_i}{\tau_{\text{xfer}}^{\text{CaATP}}}, \qquad (9)$$

$$J_{\text{xfer}}^{\text{MgATP}} = \frac{[\text{MgATP}]_{\text{ss}} - [\text{MgATP}]_i}{\tau_{\text{xfer}}^{\text{MgATP}}}. \qquad (10)$$

For the subspace, adjustment of ATP fluxes by a factor of $(V_{\text{myo}}/V_{\text{ss}})$ is necessary to account for the different volumes of myoplasm (V_{myo}) and subspace (V_{ss}).

Similar equations for the Ca^{2+} and Mg^{2+} exchange with ADP in the subspace and bulk myoplasm can be written as

$$[\text{ADP}]_{\text{ss}} = [\text{ADP}]_{\text{tot}} - [\text{CaADP}]_{\text{ss}} - [\text{MgADP}]_{\text{ss}}, \qquad (11)$$

$$\frac{d[\text{CaADP}]_{\text{ss}}}{dt} = -J_{\text{xfer}}^{\text{CaADP}}\frac{V_{\text{myo}}}{V_{\text{ss}}} + k_+^{\text{CaADP}}[\text{Ca}]_{\text{ss}}[\text{ADP}]_{\text{ss}}$$
$$- k_-^{\text{CaADP}}[\text{CaADP}]_{\text{ss}}, \qquad (12)$$

$$\frac{d[\text{MgADP}]_{\text{ss}}}{dt} = -J_{\text{xfer}}^{\text{MgADP}}\frac{V_{\text{myo}}}{V_{\text{ss}}} + k_+^{\text{MgADP}}[\text{Mg}]_{\text{ss}}[\text{ADP}]_{\text{ss}}$$
$$- k_-^{\text{MgADP}}[\text{MgADP}]_{\text{ss}}, \qquad (13)$$

$$[\text{ADP}]_i = [\text{ADP}]_{\text{tot}} - [\text{CaADP}]_i - [\text{MgADP}]_i, \qquad (14)$$

$$\frac{d[\text{CaADP}]_i}{dt} = J_{\text{xfer}}^{\text{CaADP}} + k_+^{\text{CaADP}}[\text{Ca}]_i[\text{ADP}]_i$$
$$- k_-^{\text{CaADP}}[\text{CaADP}]_i, \qquad (15)$$

$$\frac{d[\text{MgADP}]_i}{dt} = J_{\text{xfer}}^{\text{MgADP}} + k_+^{\text{MgADP}}[\text{Mg}]_i[\text{ADP}]_i$$
$$- k_-^{\text{MgADP}}[\text{MgADP}]_i. \qquad (16)$$

CaADP and MgADP fluxes (Fig. 1) are given by

$$J_{\text{xfer}}^{\text{CaADP}} = \frac{[\text{CaADP}]_{\text{ss}} - [\text{CaADP}]_i}{\tau_{\text{xfer}}^{\text{CaADP}}}, \qquad (17)$$

$$J_{\text{xfer}}^{\text{MgADP}} = \frac{[\text{MgADP}]_{\text{ss}} - [\text{MgADP}]_i}{\tau_{\text{xfer}}^{\text{MgADP}}}. \qquad (18)$$

In the model, we assume that the transfer of free and bound ATP and ADP from the subspace to the myoplasm occurs at the same rate. The changes in free Mg^{2+} concentration during excitation in the subspace are

described by

$$\frac{d[\text{Mg}]_{\text{ss}}}{dt} = -J_{\text{xfer}}^{\text{Mg}}\frac{V_{\text{myo}}}{V_{\text{ss}}} - k_+^{\text{MgATP}}[\text{Mg}]_{\text{ss}}[\text{ATP}]_{\text{ss}}$$
$$+ k_-^{\text{MgATP}}[\text{MgATP}]_{\text{ss}}$$
$$- k_+^{\text{MgADP}}[\text{Mg}]_{\text{ss}}[\text{ADP}]_{\text{ss}}$$
$$+ k_-^{\text{MgADP}}[\text{MgADP}]_{\text{ss}}, \qquad (19)$$

and in the bulk myoplasm by

$$\frac{d[\text{Mg}]_i}{dt} = J_{\text{xfer}}^{\text{Mg}} - k_+^{\text{MgATP}}[\text{Mg}]_i[\text{ATP}]_i + k_-^{\text{MgATP}}[\text{MgATP}]_i$$
$$- k_+^{\text{MgADP}}[\text{Mg}]_i[\text{ADP}]_i + k_-^{\text{MgADP}}[\text{MgADP}]_i.$$
$$(20)$$

The transfer flux of Mg^{2+} from subspace to myoplasm (Fig. 1) is given by

$$J_{\text{xfer}}^{\text{Mg}} = \frac{[\text{Mg}]_{\text{ss}} - [\text{Mg}]_i}{\tau_{\text{xfer}}^{\text{Mg}}}. \qquad (21)$$

ATP and ADP not only buffer and transport Ca^{2+} and Mg^{2+} ions but also have well-known regulatory functions in the cell (Bers, 1991; Leyssens et al., 1996; Carmeliet, 1999). In cardiac myocytes, ATP (as MgATP) drives a number of enzymes, channels (ATP-sensitive K$^+$ channels), and transporters (Na$^+$-K$^+$ ATPase pump, sarcolemmal Ca^{2+}-ATPase pump, SR Ca^{2+}-ATPase pump) (Noma, 1983; Fozzard and Lipkind, 1995; Shaw and Rudy, 1997; Yokoshiki et al., 1998; Carmeliet, 1999). To simulate transporter ATP regulation, we modified the equations of Winslow et al. (1999) for Na$^+$-K$^+$ pump current (I_{NaK}), sarcolemmal Ca^{2+} pump current ($I_{\text{p(Ca)}}$), and SR Ca^{2+} ATPase pump (J_{up}):

$$I_{\text{NaK}}^*(t) = S_{\text{MgATP}}I_{\text{NaK}}(t), \qquad (22)$$

$$I_{\text{p(Ca)}}^*(t) = S_{\text{MgATP}}I_{\text{p(Ca)}}(t), \qquad (23)$$

$$J_{\text{up}}^*(t) = S_{\text{MgATP}}J_{\text{up}}(t), \qquad (24)$$

where

$$S_{\text{MgATP}} = \frac{[\text{MgATP}]_i}{[\text{MgATP}]_{i0}}, \qquad (25)$$

and $[\text{MgATP}]_{i0}$ is the resting myoplasmic MgATP concentration in normal conditions ($[\text{ATP}]_{\text{tot}} = 7$ mM, $[\text{ADP}]_{\text{tot}} = 5$ μM, free Mg^{2+} = 1 mM).

The equations for the $[\text{Ca}]_{\text{ss}}$ and $[\text{Ca}]_i$ in the model of Winslow et al. (1999) were modified, taking into account that now ATP and ADP buffer Ca^{2+} and regulate ion

TABLE 1 Standard buffer and ionic concentrations

Definition	Symbol	Value (mM)
Total intracellular ATP concentration	$[ATP]_{tot}$	7
Total intracellular ADP concentration	$[ADP]_{tot}$	0.005
Total intracellular Mg^{2+} concentration	$[Mg]_{tot}$	7.44

pumps:

$$\frac{d[Ca]_{ss}}{dt} = \beta_{ss}\left\{ J_{rel}\frac{V_{JSR}}{V_{ss}} - J_{xfer}\frac{V_{myo}}{V_{ss}} - (I_{Ca})\frac{A_{cap}C_{sc}}{2V_{ss}F} \right.$$
$$- k_+^{CaATP}[Ca]_{ss}[ATP]_{ss} + k_-^{CaATP}[CaATP]_{ss}$$
$$\left. - k_+^{CaADP}[Ca]_{ss}\left[ADP\right]_{ss} + k_-^{CaADP}[CaADP]_{ss}\right\},$$
$$\tag{26}$$

$$\frac{d[Ca]_i}{dt} = \beta_i\left\{ J_{xfer} - J_{up}^* - J_{trpn} - (I_{Ca,b} - 2I_{NaCa} + I_{p(Ca)}^*) \right.$$
$$\times \frac{A_{cap}C_{sc}}{2V_{myo}F} - k_+^{CaATP}[Ca]_i[ATP]_i + k_-^{CaATP}[CaATP]_i$$
$$\left. - k_+^{CaADP}[Ca]_i[ADP]_i + k_-^{CaADP}[CaADP]_i\right\}, \tag{27}$$

where β_{ss} is a rapid buffering approximation factor for calmodulin in the subspace, and β_i is a rapid buffering approximation factor for calmodulin in the myoplasm.

METHODS AND MODEL PARAMETERS

The system of first-order nonlinear differential equations at given initial conditions was solved using Gill's modification of the Runge–Kutta fourth-

TABLE 2 Rate and dissociation ATP and ADP constants

Definition	Symbol	Value
Ca^{2+}-ATP dissociation constant	K_D^{CaATP}	0.1698 mM
Ca^{2+} on-rate constant for ATP	k_+^{CaATP}	225 mM^{-1} ms^{-1}
Ca^{2+} off-rate constant for ATP	k_-^{CaATP}	45 ms^{-1}
Mg^{2+}-ATP dissociation constant	K_D^{MgATP}	0.087 mM
Mg^{2+} on-rate constant for ATP	k_+^{MgATP}	125 mM^{-1} s^{-1}
Mg^{2+} off-rate constant for ATP	k_-^{MgATP}	10.875 ms^{-1}
Ca^{2+}-ADP dissociation constant	K_D^{CaADP}	1.548 mM
Ca^{2+} on-rate constant for ADP	k_+^{CaADP}	125 mM^{-1} ms^{-1}
Ca^{2+} off-rate constant for ADP	k_-^{CaADP}	193.5 ms^{-1}
Mg^{2+}-ADP dissociation constant	K_D^{MgADP}	0.676 mM
Mg^{2+} on-rate constant for ADP	k_+^{MgADP}	125 mM^{-1} ms^{-1}
Mg^{2+} off-rate constant for ADP	k_-^{MgADP}	84.5 ms^{-1}

order algorithm (Ralston and Wilf, 1960). The maximum step size for time integration was 0.1 ms and the maximum error tolerance was 10^{-6}.

Total ATP and ADP concentrations used in the model (see Table 1) are average values measured in different cardiac tissues and species (Bers, 1991; Leyssens et al., 1996; Baylor and Hollingworth, 1998; Ch'en et al., 1998). ATP and ADP dissociation constants (see Table 2) were taken from Martell and Smith (1982), and Kargacin and Kargacin (1997). The on- and off-rate constants, k_+^{CaATP} and k_-^{CaATP}, were obtained from Baylor and Hollingworth (1998). We could not find published data for the values of CaADP, MgATP, and MgADP on- and off-rate binding parameters. Therefore, the typical near-diffusion-limited on-rate value of 125 μM^{-1} s^{-1} has been assumed (see Table 2) (Soeller and Cannell, 1997; Ch'en et al., 1998). The corresponding off-rate constants were obtained from the known values of equilibrium dissociation constants (K_D^{CaADP}, K_D^{MgATP}, K_D^{MgADP}).

It is known that free Mg^{2+} in cardiac cells is between 0.5 and 2 mM (Bers, 1991; Leyssens et al., 1996; Carmeliet, 1999; Murphy et al., 1989). Here we assume that, at equilibrium, free Mg^{2+} concentrations in the subspace and myoplasm do not differ, a value of 1 mM was used for both (see Table 3). Total Mg^{2+} concentration ($\sim$7.44 mM) was estimated from

TABLE 3 Initial conditions

Definition	Symbol	Value
Time	t	0 ms
Free subspace ATP concentration	$[ATP]_{ss}$	0.56 mM
Subspace concentration of Ca^{2+}-bound ATP	$[CaATP]_{ss}$	0.25×10^{-3} mM
Subspace concentration of Mg^{2+}-bound ATP	$[MgATP]_{ss}$	6.4395 mM
Free myoplasmic ATP concentration	$[ATP]_i$	0.56 mM
Myoplasmic concentration of Ca^{2+}-bound ATP	$[CaATP]_i$	0.237×10^{-3} mM
Myoplasmic concentration of Mg^{2+}-bound ATP	$[MgATP]_i$	6.4395 mM
Free subspace ADP concentration	$[ADP]_{ss}$	0.002 mM
Subspace concentration of Ca^{2+}-bound ADP	$[CaADP]_{ss}$	0.13×10^{-6} mM
Subspace concentration of Mg^{2+}-bound ADP	$[MgADP]_{ss}$	0.298×10^{-2} mM
Free myoplasmic ADP concentration	$[ADP]_i$	0.002 mM
Myoplasmic concentration of Ca^{2+}-bound ADP	$[CaADP]_i$	0.11×10^{-6} mM
Myoplasmic concentration of Mg^{2+}-bound ADP	$[MgADP]_i$	0.298×10^{-2} mM
Free subspace Mg^{2+} concentration	$[Mg]_{ss}$	1 mM
Free myoplasmic Mg^{2+} concentration	$[Mg]_i$	1 mM
Free subspace Ca^{2+} concentration	$[Ca]_{ss}$	1.315×10^{-4} mM
Free myoplasmic Ca^{2+} concentration	$[Ca]_i$	8.464×10^{-5} mM
JSR Ca^{2+} concentration	$[Ca]_{JSR}$	0.2616 mM
NSR Ca^{2+} concentration	$[Ca]_{NSR}$	0.2620 mM
Intracellular Na^+ concentration	$[Na]_i$	10 mM
Intracellular K^+ concentration	$[K]_i$	159.48 mM

TABLE 4   Time constants

Definition	Symbol	Value (ms)
Time constant for transfer of CaATP from subspace to myoplasm	$\tau_{\text{xfer}}^{\text{CaATP}}$	53.4
Time constant for transfer of MgATP from subspace to myoplasm	$\tau_{\text{xfer}}^{\text{MgATP}}$	53.4
Time constant for transfer of CaADP from subspace to myoplasm	$\tau_{\text{xfer}}^{\text{CaADP}}$	53.4
Time constant for transfer of MgADP from subspace to myoplasm	$\tau_{\text{xfer}}^{\text{MgADP}}$	53.4
Time constant for transfer of Mg from subspace to myoplasm	$\tau_{\text{xfer}}^{\text{Mg}}$	26.7

the accepted free Mg^{2+} concentration of 1 mM at ~100 nM free Ca^{2+}. We also assumed that total Mg^{2+} concentration in the cell remains constant, while free Mg^{2+} concentration varies with concentration of total ATP and ADP as Ca^{2+} and Mg^{2+} buffers. The Mg^{2+} transfer-time constant from the subspace to the myoplasm (see Table 4) was chosen to be equal to the Ca^{2+} transfer-time constant (τ_{xfer}) used by Winslow et al. (1999). The transfer of free and bound ATP and ADP was assumed to occur at half the rate of free Ca^{2+} and Mg^{2+} diffusion (see Table 4) (Baylor and Hollingworth, 1998). Unless specified otherwise in the figure legends or in the text, the standard set of parameters and initial conditions used in the calculations is listed in the Tables. All other initial conditions and values of the parameters that are not included in the Tables correspond to those listed in the Appendix of Winslow et al. (1999).

In this paper, the effects of ATP and ADP buffering, transport, and regulation in normal conditions and during metabolic inhibition were examined in response to periodic voltage-clamp stimuli (−97 mV holding potential, 3 mV step potential, 200 ms duration) at a frequency of 1 Hz.

RESULTS

Ion and buffer concentrations and ion currents in normal conditions

Ca^{2+}, Na$^+$, K$^+$ concentrations and ion currents with inclusion of Mg^{2+}, ATP, and ADP

Here we report the results of several simulations, investigating how including 1 mM Mg^{2+}, 7 mM ATP, and 5 μM ADP may contribute to the amplitude and time course of intracellular Ca^{2+}, Na$^+$, and K$^+$ transients and ion currents.

In the first set of simulations, [Ca]$_{\text{ss}}$ and [Ca]$_i$ (10th cycle, 9–10 s) were calculated according to the approximation of Winslow et al. (1999), i.e., without Mg^{2+}, ATP, and ADP included. The solid lines in Fig. 2, *A* and *B*, show that [Ca]$_{\text{ss}}$ reached a peak of ~30 μM after ~4 ms, whereas [Ca]$_i$ reached a peak of ~0.54 μM after ~48 ms. As shown in Fig. 2 *C* (*solid line*), JSR was almost depleted during Ca^{2+} release. The change in [Ca]$_{\text{JSR}}$ from a diastolic level of ~229 μM to ~83 μM was ~64%.

In the second set of simulations, ATP and ADP were treated as stationary buffers to examine the effects of Ca^{2+} and Mg^{2+} exchange with ATP and ADP. In the subspace, [Ca]$_{\text{ss}}$ time course was not affected (dashed line in Fig. 2 *A* coincides with solid line) whereas, in the myoplasm, Ca^{2+} concentration had a slightly reduced amplitude (Fig. 2 *B*, dashed line). In addition, these calculations demonstrated

that the changes in Ca^{2+} concentrations are mainly due to Ca^{2+} and Mg^{2+} binding by ATP. Neither [Ca]$_{\text{ss}}$ nor [Ca]$_i$ time courses (Fig. 2 *A*, solid or dashed lines; Fig. 2 *B*, dashed line) were affected by changes in total ADP concentration from 0 μM to 100 μM.

Including 1 mM Mg^{2+}, 7 mM ATP, and 5 μM ADP in the model did not affect JSR Ca^{2+} concentration levels or the L-type Ca^{2+} current (Fig. 2, *C* and *D*, solid and dashed lines coincide). [Na]$_i$ and I_{Na} current were influenced to some extent, but not notably (not shown). [K]$_i$, I_{NaCa}, $I_{\text{p(Ca)}}^*$, $I_{\text{Ca,K}}$, $I_{\text{Ca,b}}$, I_{Kr}, I_{Ks}, I_{to1}, I_{K1}, I_{Kp}, I_{NaK}^*, and $I_{\text{Na,b}}$ remained unchanged after adding Mg^{2+}, ATP, and ADP.

To study the significance of the mobility of Mg^{2+}, ATP, and ADP in determining Ca^{2+}, Na$^+$, and K$^+$ concentrations and ion currents, we performed another set of calculations, including initially only $J_{\text{xfer}}^{\text{CaATP}}$. The outputs of the model (10th cycle, 9–10 s) in response to rhythmically applied clamp pulses are shown in Fig. 2 (dotted lines). Figure 2 *A* shows that [Ca]$_{\text{ss}}$ amplitude decreased and [Ca]$_{\text{ss}}$ relaxation slightly accelerated when $J_{\text{xfer}}^{\text{CaATP}}$ was included. Additionally, the simulations demonstrated that the changes in [Ca]$_{\text{ss}}$ transient slightly affected the time course of I_{Ca} (Fig. 2 *D*, dotted line). Figure 2 *C* (dotted line) shows that the diastolic JSR Ca^{2+} level was elevated and that the JSR was less depleted after the inclusion of $J_{\text{xfer}}^{\text{CaATP}}$. The model results (Fig. 2 *C*, dotted line) also showed that the JSR is again almost ⅔ depleted (~62%) by a single beat. Including $J_{\text{xfer}}^{\text{CaATP}}$ elevated the stationary [Ca]$_i$ peak (Fig. 2 *B*, compare dashed and dotted lines). However, the simulation indicated that, under normal conditions, ATP and ADP buffering and transport has a negligible effect on the [Ca]$_i$ transient (Fig. 2 *B*, solid and dotted lines almost coincide). Including $J_{\text{xfer}}^{\text{CaATP}}$ resulted in small changes in the stationary [Na]$_i$ and I_{Na} time courses (10th cycle, 9–10 s) while [K]$_i$, I_{NaCa}, $I_{\text{p(Ca)}}^*$, $I_{\text{Ca,K}}$, $I_{\text{Ca,b}}$, I_{Kr}, I_{Ks}, I_{to1}, I_{K1}, I_{Kp}, I_{NaK}^*, and $I_{\text{Na,b}}$ currents remained essentially unchanged (not shown). The calculations also indicated that adding other fluxes ($J_{\text{xfer}}^{\text{Mg}}$, $J_{\text{xfer}}^{\text{CaADP}}$, $J_{\text{xfer}}^{\text{MgATP}}$, $J_{\text{xfer}}^{\text{MgADP}}$) had no observable influence on [Ca]$_{\text{ss}}$, [Ca]$_i$, and [Ca]$_{\text{JSR}}$ (Fig. 2, *A–C*, dotted lines), or on [Na]$_i$ and [K]$_i$ transients and ion currents.

Free and bound Mg^{2+}, ATP, and ADP concentrations in the presence and absence of fluxes

Kargacin and Kargacin (1997) reported that, during excitation in smooth muscle cells, the high Ca^{2+} signal near the membrane might significantly influence free subspace ATP concentration in contrast to the negligible changes in free myoplasmic ATP concentration stimulated by the low myoplasmic Ca^{2+} signal. Our simulations in ventricular myocytes showed that high subspace Ca^{2+} concentrations indeed caused more sensitive changes in the [ATP]$_{\text{ss}}$ than the low Ca^{2+} signal stimulated in [ATP]$_i$. However, these changes were not as significant as they were in smooth muscle cells (in smooth muscle cells, rest ATP was ~70
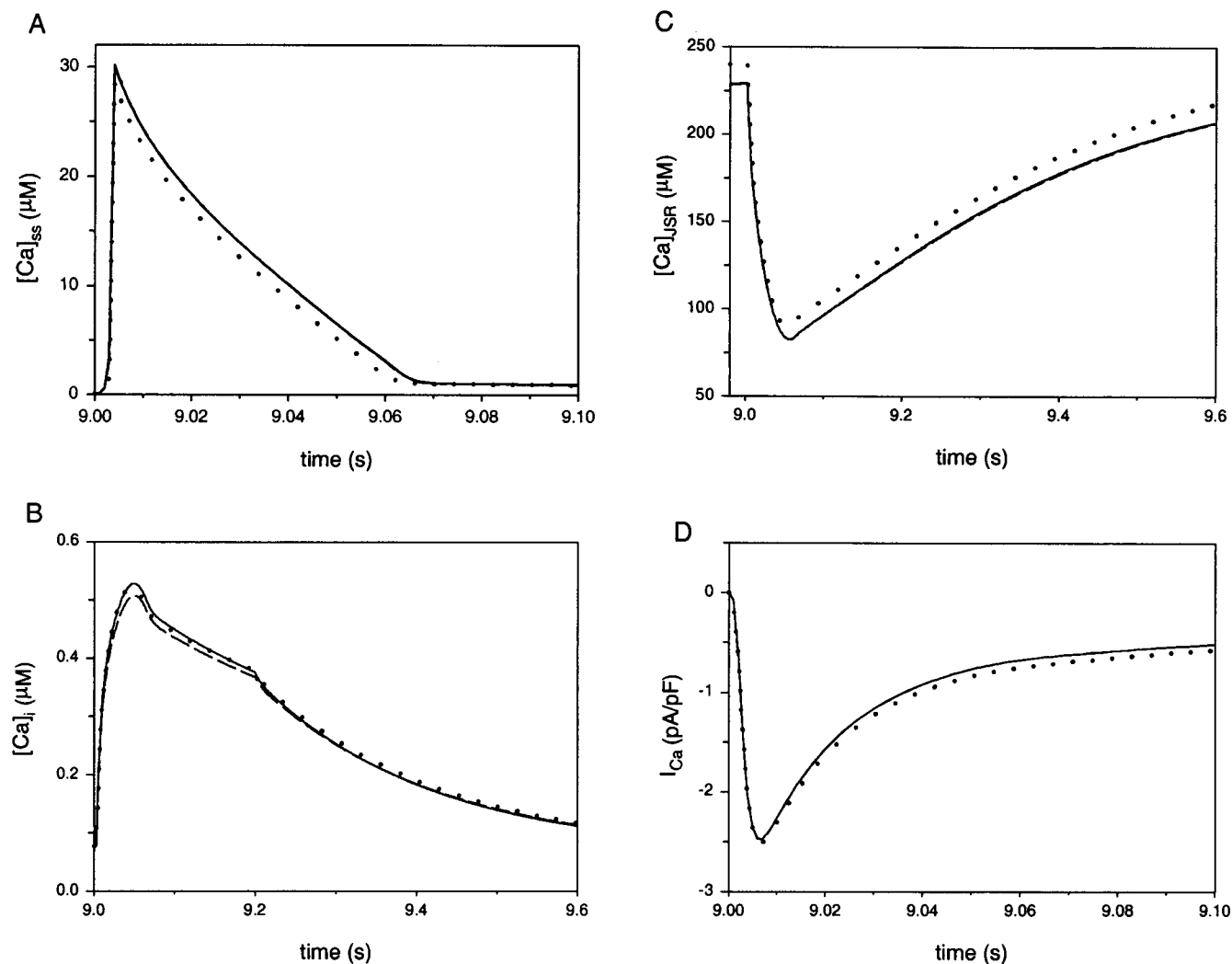
A

C

B

D

FIGURE 2   Model outputs in response to 1-Hz periodic voltage-clamp pulse of −97 mV holding potential, 3 mV step potential, and 200 ms duration. Only responses to the 10th stimulus (9–10 s) are shown. (*A*) Subspace Ca^{2+} transient. (*B*) Myoplasmic Ca^{2+} transient. (*C*) JSR Ca^{2+} transient. (*D*) L-type Ca^{2+} current. Mg^{2+}, ATP, and ADP not included (solid line). ATP and ADP treated as stationary buffers (dashed line). CaATP flux or all fluxes included (dotted line). For simulations (dashed and dotted lines) $[ATP]_{tot} = 7$ mM, $[ADP]_{tot} = 5$ μM, free $Mg^{2+} = 1$ mM. In all simulations shown, $[Mg]_{tot} = 7.44$ mM, $[K]_0 = 4$ mM, $[Na]_0 = 138$ mM, $[Ca]_0 = 2$ mM.

μM whereas, in ventricular myocytes, rest ATP was ~560 μM). During excitation, free $[ATP]_{ss}$ and $[ATP]_i$ (10th cycle, 9–10 s) decreased from the initial level by ~30.5 μM and by ~0.477 μM, respectively, when ATP and ADP were treated as stationary buffers (Fig. 3, *A* and *B*, dashed lines). The inclusion of Mg^{2+}, ATP, and ADP fluxes (Fig. 3, *A* and *B*, dotted lines) decreased the diastolic $[ATP]_{ss}$ level by ~6.24 μM and the diastolic $[ATP]_i$ level by ~0.484 μM.

Numerical studies also showed that, as free ATP concentration (10th cycle, 9–10 s) falls during excitation, free Mg^{2+} concentration rises, but not notably. Systolic $[Mg]_{ss}$ increased from the diastolic level of 1 mM by 49.3 and 1.1 μM and systolic $[Mg]_i$ by 0.75 and 0.72 μM with ATP and ADP stationary or mobile (not shown).

Most notably, the changes in $[Ca^{2+}]_{ss}$ from ~0.1 to ~30 μM (10th cycle, 9–10 s) influenced $[CaATP]_{ss}$. $[CaATP]_{ss}$

increased from 0.22 μM up to ~80 μM in the absence, and up to ~8.25 μM in the presence of fluxes. The changes in $[Ca^{2+}]_i$ from ~0.1 to ~0.53 μM did not strongly influence $[CaATP]_i$. $[CaATP]_i$ increased from 0.22 μM up to ~1.42 μM (ATP and ADP stationary) and up to ~1.466 μM (ATP and ADP mobile). In contrast to the notable changes in $[CaATP]_{ss}$, the changes in $[MgATP]_{ss}$ were small and not as significant as in smooth muscle cells (Kargacin and Kargacin, 1997). Systolic $[MgATP]_{ss}$ decreased by ~49 μM from the initial level of 6.44 mM (ATP and ADP stationary) and by ~1.8 μM in the presence of fluxes. Model studies also suggested that, under normal conditions (7 mM ATP, 5 μM ADP, and 1 mM free Mg^{2+}), changes in systolic $[MgATP]_i$ concentration (10th cycle, 9–10 s) are negligible. $[MgATP]_i$ dropped by ~0.75 μM from the initial level of 6.44 mM

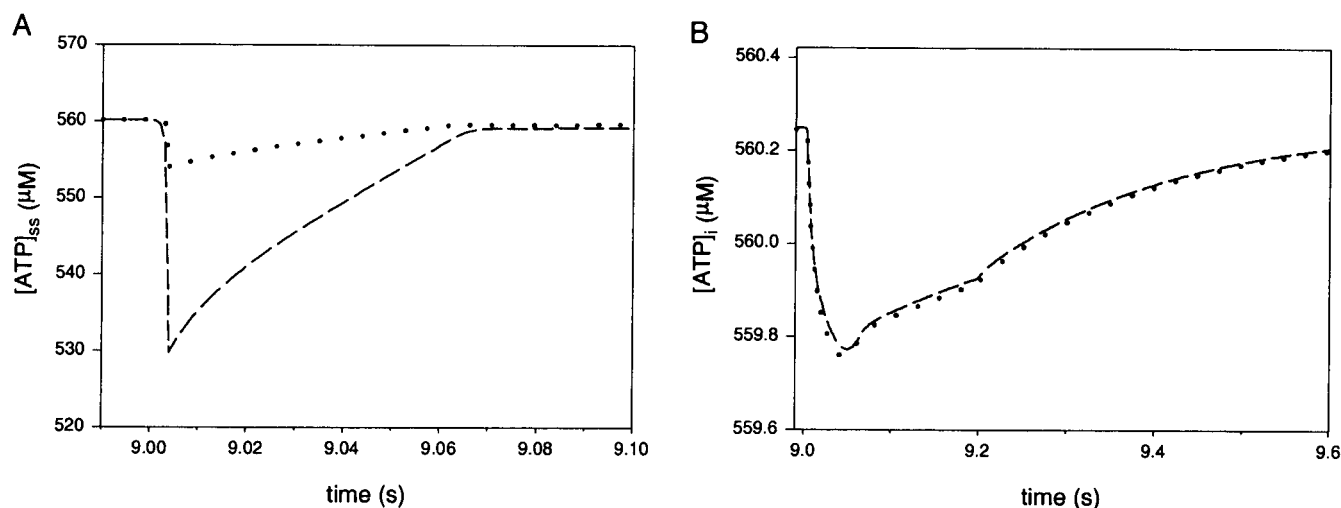FIGURE 3   (A) Effect of changes in subspace Ca^{2+} concentration on free subspace ATP concentration and (B) of changes in myoplasmic Ca^{2+} concentration on free myoplasmic ATP concentration. ATP and ADP treated as stationary buffers (dashed line). All fluxes included (dotted line). Only responses to the 10th voltage-clamp stimulus (-97 mV holding potential, 3 mV step potential, 200 ms duration, frequency 1 Hz) are shown. [ATP]$_{tot}$ = 7 mM, [ADP]$_{tot}$ = 5 μM, free Mg^{2+} = 1 mM.

when ATP and ADP were treated as either stationary or mobile.

Changes in the systolic [Ca]$_{ss}$ transient (Fig. 2 A) also stimulated a decrease of 0.036% (ATP and ADP stationary) and a decrease of 0.0003% (mobile ATP and ADP) in [ADP]$_{ss}$, while [ADP]$_i$ remained almost unchanged. Under normal conditions, the increase in systolic [CaADP]$_{ss}$ and [CaADP]$_i$ concentrations (10th cycle, 9–10 s) from the initial diastolic level of ~0.1 nM was also negligible. Surprisingly, the time courses of [MgADP]$_{ss}$ and [MgADP]$_i$ demonstrated an interesting behavior in the presence and absence of the fluxes. Dur-

ing excitation, [MgADP]$_{ss}$ and [MgADP]$_i$ rose when ATP and ADP were treated as stationary buffers (Fig. 4, A and B, dashed lines) in contrast to [MgATP]$_{ss}$ and [MgATP]$_i$, which decreased (not shown). Another interesting result was that the fluxes were able to invert the stationary [MgADP]$_{ss}$ time course (Fig. 4 A, dotted line) but were not able to invert the stationary [MgADP]$_i$ time course (Fig. 4 B, dotted line).

Calculations also indicated that high Ca^{2+} concentrations developed near the cell membrane (10th cycle, 9–10 s) increased the resting [CaATP]$_{ss}$/[MgATP]$_{ss}$ ratio ~250-fold (stationary ATP and ADP) or ~36-fold (mobile ATP and
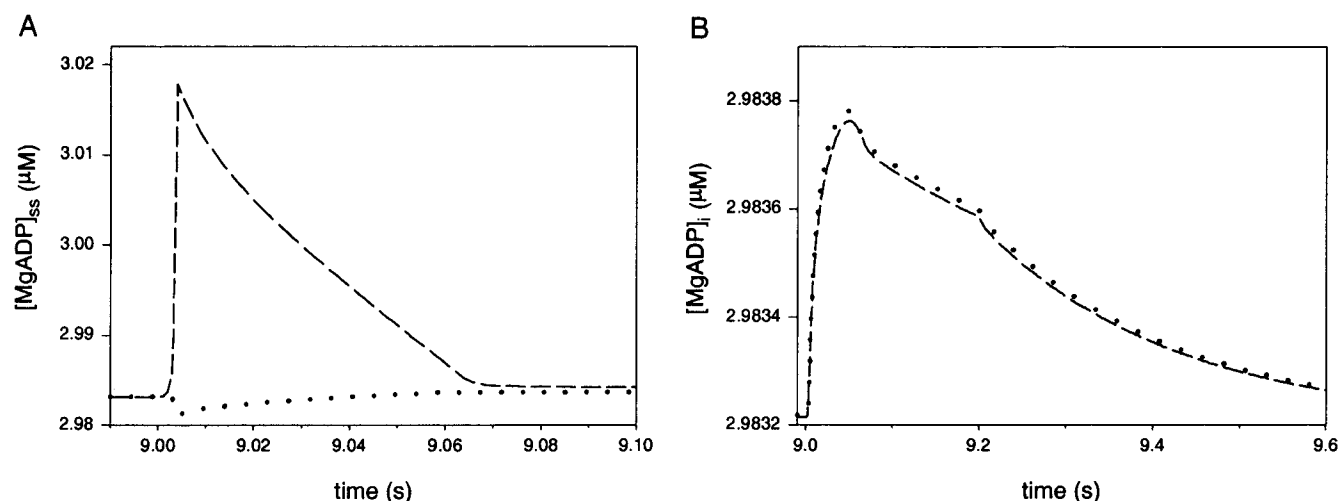

FIGURE 4   Time courses of MgADP (9–10 s) in (A) subspace and (B) myoplasm. ATP and ADP treated as stationary buffers (dashed line). All fluxes included (dotted line). Simulations are generated in response to 1-Hz voltage-clamp pulse (-97 mV holding potential, 3 mV step potential, 200 ms duration). [ATP]$_{tot}$ = 7 mM, [ADP]$_{tot}$ = 5 μM, free Mg^{2+} = 1 mM.

ADP). [CaATP]$_i$/[MgATP]$_i$ ratio increased ~6.87-fold with ATP and ADP stationary or mobile. Changes in free Ca^{2+} concentrations over the range of 0.1 to ~30 μM did not affect the subspace or myoplasmic high-energy phosphate ratio (MgADP/MgATP). In smooth muscle cells, Kargacin and Kargacin (1997) also predicted significant changes in CaATP/MgATP concentration ratio and no alterations in MgADP/MgATP ratio during cell excitation.

Ion and buffer concentrations, and ion currents during metabolic inhibition

Experimental studies have demonstrated that block of oxidative metabolism and a fall in [ATP]$_{tot}$/[ADP]$_{tot}$ ratio cause important changes in ion concentrations ([K$^+$]$_0$, [H$^+$]$_i$, [Na$^+$]$_i$, [Ca^{2+}]$_i$, [Mg^{2+}]$_i$) and have important effects on channels and carriers (Murphy et al., 1989; Marban et al., 1990; Wagner et al., 1990; Isenberg et al., 1993; Wilde and Aksnes, 1995; Carmeliet, 1999; Huser et al., 2000). Ch'en et al. (1998) reported that, while creatine phosphate is present, total ATP and ADP concentrations remain constant, at ~7 and ~0 mM, respectively. Once ATP is depleted, ADP starts to increase, and, after ~460 s, total ATP and ADP levels become approximately equal (~3 mM) during ischemia. Taking these results into consideration, we calculated ion and buffer concentrations and simulated ion currents when [ATP]$_{tot}$ and [ADP]$_{tot}$ were 3 mM and mobile. Initial free Mg^{2+} concentrations ($t = 0$ s) in the subspace and myoplasm ([Mg]$_{ss}$, [Mg]$_i$) were estimated to be ~2.248 mM, assuming that total intracellular Mg^{2+} concentration remains constant (7.44 mM) after the fall in [ATP]$_{tot}$/[ADP]$_{tot}$ ratio from 1400 (normal conditions) to unity. During these simulations, the initial free and bound metabolic ATP and ADP concentrations were [ATP]$_{ss}$ = 112 μM, [CaATP]$_{ss}$ = 0.05 μM, [MgATP]$_{ss}$ = 2.888 mM, [ATP]$_i$ = 112 μM, [CaATP]$_i$ = 0.047 μM, [MgATP]$_i$ = 2.888 mM, [ADP]$_{ss}$ = 694 μM, [CaADP]$_{ss}$ = 0.045 μM, [MgADP]$_{ss}$ = 2.3 mM, [ADP]$_i$ = 694 μM, [CaADP]$_i$ = 0.038 μM, and [MgADP]$_i$ = 2.3 mM. Under metabolic conditions for the period of 10 s stimulation, the extracellular concentrations of K$^+$, Na$^+$, and Ca^{2+} were kept constant at normal values ([K]$_0$ = 4 mM, [Na]$_0$ = 138 mM, and [Ca]$_0$ = 2 mM). All other initial conditions and values of the parameters used were those listed in our Tables and in the Appendix of Winslow et al. (1999).
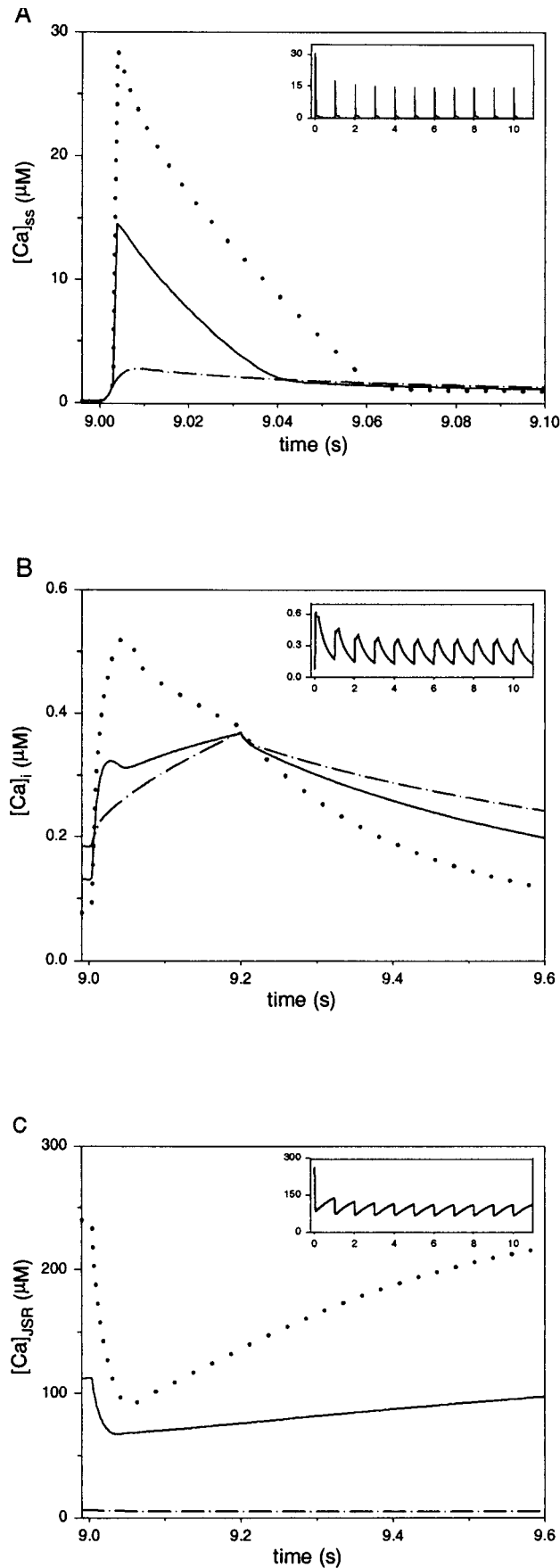
Ca^{2+}, Na$^+$, K$^+$ concentrations and ion currents

The results demonstrated that a fall in [ATP]$_{tot}$/[ADP]$_{tot}$ ratio produced significant changes in intracellular Ca^{2+} concentrations and ion currents (I_{Ca}, I_{NaCa}, I^*_{NaK}, $I^*_{p(Ca)}$), calculated in response to a periodic voltage-clamp stimuli with 200-ms duration and -97 mV and 3 mV holding and step potentials.

Figure 5 C (top trace) shows that, following the first stimulus, [Ca^{2+}]$_{JSR}$ load is greatly reduced when [ATP]$_{tot}$ and [ADP]$_{tot}$ were each 3 mM. This significantly decreased the [Ca]$_{ss}$ transient and increased I_{Ca} during the subsequent stimulus (Fig. 5 A and Fig. 6 A, top traces). Figure 5, B and C (top traces), also show that increased I_{Ca} was not able to increase the [Ca]$_i$ transient or [Ca^{2+}]$_{JSR}$ loading. The [Ca]$_{ss}$, [Ca]$_i$, and [Ca]$_{JSR}$ transients continued to decline. Figure 5 A (9–10 s, solid line) shows that normal [Ca]$_{ss}$ amplitude dropped ~50% and that the pathological [Ca]$_{ss}$ transient reached the diastolic level earlier than the normal [Ca]$_{ss}$. Figure 5 B (9–10 s, solid line) shows that the normal [Ca]$_i$ peak also decreased ~50% and that a second higher slow peak appeared. In contrast to accelerated [Ca]$_{ss}$ relaxation (Fig. 5 A, solid line), the pathological [Ca]$_i$ transient decayed more slowly than normal. The model also predicted that diastolic [Ca]$_i$ (~0.13 μM) and diastolic [Ca]$_{ss}$ (~0.15 μM) levels reached during metabolic inhibition were higher than those under normal conditions. Figure 5 C (9–10 s, solid line) shows that less Ca^{2+} was stored in the junctional SR after a fall in [ATP]$_{tot}$/[ADP]$_{tot}$ ratio. The pathological [Ca^{2+}]$_{JSR}$ level was more depleted and the recovery of [Ca]$_{JSR}$ was more delayed than under normal conditions. In response to 1-Hz voltage-clamp pulses after 10 s, intracellular [Na]$_i$ increased by ~0.33 mM, whereas the intracellular [K]$_i$ decreased slightly (~0.13 mM).

The model also predicted that a fall in [ATP]$_{tot}$/[ADP]$_{tot}$ ratio has an important modulatory effect on the ion currents and carriers. Figure 6 A (9–10 s, solid line) shows that the decreased [Ca]$_{ss}$ transient caused notable increase in L-type Ca^{2+} current (I_{Ca}). Changes in systolic [Ca]$_i$, [Na]$_i$, [K]$_i$ and diastolic [MgATP]$_i$ concentrations during metabolic inhibition had pronounced effects on I_{NaCa}, I^*_{NaK}, and $I^*_{p(Ca)}$ as well (Fig. 6, B–D, solid lines). The simulations demonstrated that the time courses of $I_{Ca,K}$, $I_{Ca,b}$, I_{Na}, I_{K1}, and $I_{Na,b}$ (10th cycle, 9–10 s) were also influenced to some extent (not shown). Because extracellular K$^+$ and Na$^+$ concentrations were kept constant ([K]$_0$ = 4 mM, [Na]$_0$ = 138 mM) and alterations in [K]$_i$ and [Na]$_i$ were small, the calculated I_{Kr}, I_{Ks}, I_{to1}, and I_{Kp} remained unchanged.

Ch'en et al. (1998) reported that, after ~550 s simulated ischemia, total ATP and ADP levels become approximately zero. In the present study, we also calculated ion concentrations and currents when [ATP]$_{tot}$ and [ADP]$_{tot}$ were 0 mM (total metabolic inhibition). During this set of simulations, the initial free Mg^{2+} concentrations ($t = 0$ s) in the subspace and myoplasm were 7.44 mM and all initial free and bound ATP and ADP concentrations were zero. With total metabolic inhibition, the model predicted that (Figs. 5 and 6, dash-dot lines): 1) the SR is almost depleted; 2) diastolic Ca^{2+} levels are further increased; 3) systolic Ca^{2+} levels continued decreasing; 4) an earlier [Ca]$_i$ peak disappeared; 5) the L-type Ca^{2+} influx further increased, while Na$^+$/Ca^{2+} exchanger efficiency decreased; 6) Na$^+$-K$^+$ cur-

rent and sarcolemmal Ca^{2+} current are totally blocked; and 7) $[Na^+]_i$ slightly increased, while $[K^+]_i$ slightly decreased.

Free and bound Mg²⁺, ATP, and ADP concentrations

To estimate the effect of metabolic inhibition on the free and bound Mg^{2+}, ATP, and ADP concentrations, we computed these concentrations in response to 10 current pulses delivered at a frequency of 1 Hz.

Figure 7, A and B, shows that diastolic $[ATP]_{ss}$ and $[ATP]_i$ dropped ~5-fold when total ATP and ADP were 3 mM and free Mg^{2+} was 2.248 mM. Systolic $[ATP]_{ss}$ decreased from 111.77 to 111.3 μM (Fig. 7 A), whereas, in normal conditions, $[ATP]_{ss}$ dropped from 560.2 to 554 μM (Fig. 3 A, dotted line). Systolic $[ATP]_i$ remained almost unchanged, dropped only by ~14 nM (Fig. 7 B). Figure 7 B also demonstrates that a fall in $[ATP]_{tot}/[ADP]_{tot}$ gave rise to a second slow peak in the $[ATP]_i$ transient (compare with Fig. 3 B, dotted line).

Diastolic $[Mg]_{ss}$ and $[Mg]_i$ rose ~2.25-fold during metabolic inhibition. Systolic $[Mg]_{ss}$ and $[Mg]_i$ (10th cycle, 9–10 s) increased by ~0.5 and ~0.17 μM from the resting level of 2.248 mM. In normal conditions, diastolic Mg^{2+} concentration was 1 mM and $[Mg]_{ss}$ and $[Mg]_i$ increased by ~1.1 and ~0.75 μM, respectively. Simulations also demonstrated that a reduction of $[ATP]_{tot}/[ADP]_{tot}$ caused a second slow peak in the $[Mg]_i$ transient to appear (not shown).

Calculated diastolic CaATP concentrations (10th cycle, 9–10 s) were ~70% less than normal. Systolic $[CaATP]_{ss}$ and $[CaATP]_i$ increased by ~0.8 and ~0.125 μM from the initial level of 74 nM when $[ATP]_{tot}/[ADP]_{tot}$ was one. The increase in normal systolic $[CaATP]_{ss}$ and $[CaATP]_i$ from the initial level of 224 nM was ~8 and 1.24 μM, respectively. These studies also demonstrated that a second slow peak in the pathological $[CaATP]_i$ transient appeared. The fall in $[ATP]_{tot}/[ADP]_{tot}$ ratio decreased diastolic $[MgATP]_{ss}$ and $[MgATP]_i$ from 6.44 to ~2.888 mM. Simulations also showed that the changes in systolic $[MgATP]_{ss}$ and $[MgATP]_i$ (10th cycle, 9–10 s) were again negligible, as under normal conditions. Systolic $[MgATP]_{ss}$ concentration decreased by ~0.3 μM from the initial level of 2.888 mM. Systolic $[MgATP]_i$ dropped by ~0.125 μM. Under

FIGURE 5   Model outputs in response to 1-Hz periodic voltage-clamp pulse of −97 mV holding potential, 3 mV step potential, and 200 ms duration. (A) Subspace Ca^{2+} transient (9–10 s). (B) Myoplasmic Ca^{2+} transient (9–10 s). (C) JSR Ca^{2+} transient (9–10 s). ATP and ADP are treated as mobile Ca^{2+} and Mg^{2+} buffers. $[ATP]_{tot} = 7$ mM, $[ADP]_{tot} = 5$ μM, free $Mg^{2+} = 1$ mM (dotted line). $[ATP]_{tot} = 3$ mM, $[ADP]_{tot} = 3$ mM, free $Mg^{2+} = 2.248$ mM (solid line). $[ATP]_{tot} = 0$ mM, $[ADP]_{tot} = 0$ mM, free $Mg^{2+} = 7.44$ mM (dash-dot line). Top traces in (A), (B), and (C) show $[Ca]_{ss}$, $[Ca]_i$, and $[Ca]_{JSR}$ transients during metabolic inhibition ($[ATP]_{tot} = [ADP]_{tot} = 3$ mM, free $Mg^{2+} = 2.248$ mM) for the period 0–11 s.
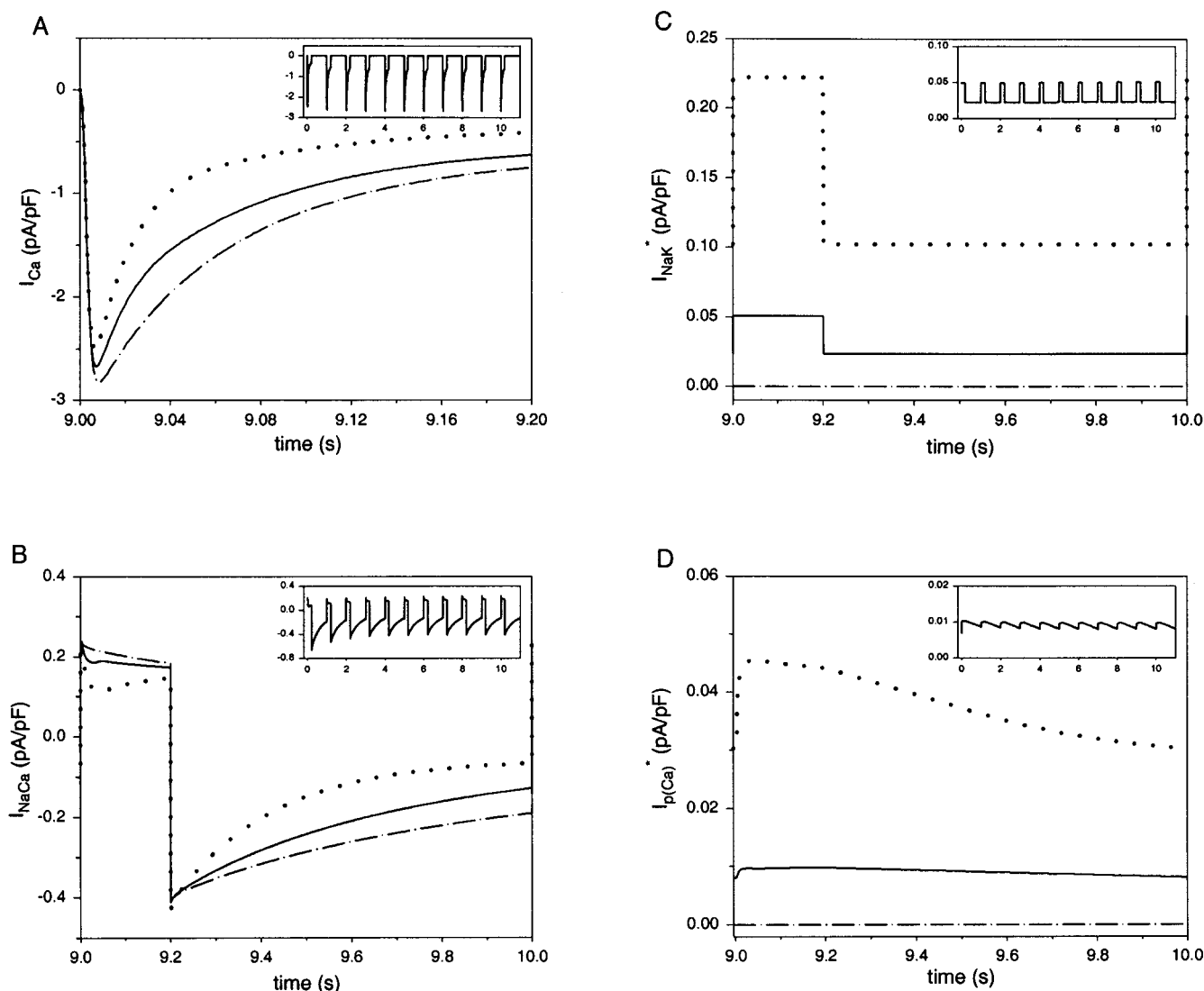
FIGURE 6   Model simulations for a periodic voltage-clamp pulse of −97 mV holding potential, 3 mV step potential, 200 ms duration, frequency 1 Hz. (A) L-type Ca^{2+} current. (B) Na^+-Ca^{2+} exchange current. (C) Na^+-K^+ pump current. (D) Sarcolemmal Ca^{2+} pump current. ATP and ADP are treated as mobile Ca^{2+} and Mg^{2+} buffers. $[ATP]_{tot} = 7$ mM, $[ADP]_{tot} = 5$ μM, free $Mg^{2+} = 1$ mM (dotted line). $[ATP]_{tot} = 3$ mM, $[ADP]_{tot} = 3$ mM, free $Mg^{2+} = 2.248$ mM (solid line). $[ATP]_{tot} = 0$ mM, $[ADP]_{tot} = 0$ mM, free $Mg^{2+} = 7.44$ mM (dash-dot line). Top traces in (A), (B), (C), and (D) show I_{Ca}, I_{NaCa}, I_{NaK}^*, and $I_{p(Ca)}^*$ with metabolic inhibition ($[ATP]_{tot} = [ADP]_{tot} = 3$ mM, free $Mg^{2+} = 2.248$ mM) for the period 0–11 s.

normal conditions, systolic $[MgATP]_{ss}$ and $[MgATP]_i$ increased by ~1.8 and ~0.75 μM from the level of 6.44 mM. A second late peak in the $[MgATP]_i$ transient emerged when $[ATP]_{tot}/[ADP]_{tot}$ was unity.

Calculations showed that diastolic $[ADP]_{ss}$ and $[ADP]_i$ increased ~345-fold when total ATP and ADP were 3 mM and free Mg^{2+} was 2.248 mM. Subspace ADP concentration (10th cycle, 9–10 s) decreased by ~1.38 μM from the diastolic pathological level of 693.55 μM as long as normal $[ADP]_{ss}$ dropped by ~10 nM from the normal diastolic level of 2.017 μM. Changes in the pathological and normal myoplasmic ADP concentrations were negligible. Pathological $[ADP]_i$ dropped by ~60 nM whereas normal $[ADP]_i$

dropped by ~1.2 nM. Model simulations demonstrated that a late second peak in $[ADP]_i$ transient also emerged when $[ATP]_{tot}/[ADP]_{tot}$ was unity.

The calculated diastolic CaADP concentrations were ~500-fold higher than normal. Systolic $[CaADP]_{ss}$ (9–10 s) increased by ~2.3 μM and systolic $[CaADP]_i$ by ~0.11 μM from the initial level of 50 nM during metabolic inhibition. The increase in normal systolic $[CaADP]_{ss}$ and $[CaADP]_i$ from the initial level of 0.1 nM was negligible. Diastolic $[MgADP]_{ss}$ and $[MgADP]_i$ rose from ~3 μM up to ~2.3 mM. In addition, simulations showed that the changes in systolic $[MgADP]_{ss}$ and $[MgADP]_i$ concentrations (9–10 s) were again negligible. A second slow peak in
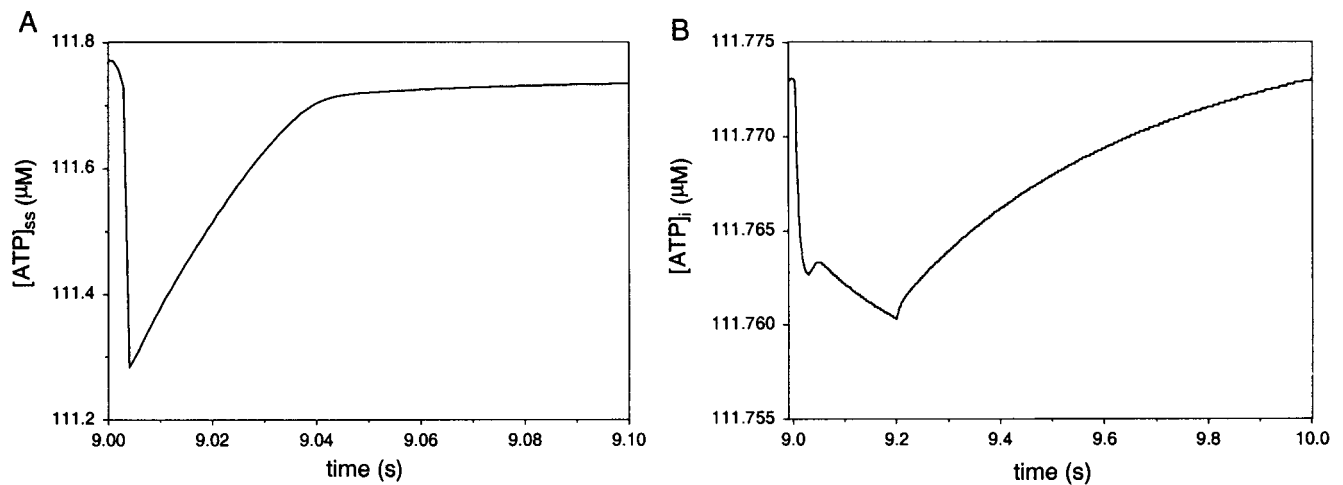
FIGURE 7   (A) Effect of changes in subspace Ca^{2+} concentration on free subspace ATP concentration, and (B) of changes in myoplasmic Ca^{2+} concentration on free myoplasmic ATP concentration with metabolic inhibition ([ATP]$_{tot}$ = 3 mM, [ADP]$_{tot}$ = 3 mM, free Mg^{2+} = 2.248 mM). Simulations are generated in response to 1-Hz voltage-clamp pulse (−97 mV holding potential, 3 mV step potential, 200 ms duration). ATP and ADP are treated as mobile Ca^{2+} and Mg^{2+} buffers.

pathological [CaADP]$_i$ and [MgADP]$_i$ transients also appeared. Another interesting model result was that 3 mM [ATP]$_{tot}$ and 3 mM [ADP]$_{tot}$ were able to stimulate systolic [MgADP]$_i$ to decrease (not shown) in contrast to the increased [MgADP]$_i$ seen in normal conditions (Fig. 4 B, dotted line).

Because total ATP concentration dropped and total ADP concentration rose, the importance of CaADP flux (J_{xfer}^{CaADP}) in transporting Ca^{2+} from the subspace to the myoplasm increased while the importance of CaATP flux (J_{xfer}^{CaATP}) decreased. The model studies demonstrated that, during metabolic inhibition, systolic [Ca]$_{ss}$ amplitude decreased and [Ca]$_{ss}$ relaxation slightly accelerated only when J_{xfer}^{CaADP} was included. Systolic time courses of [Ca]$_{ss}$ (or [Ca]$_i$) remained unchanged when the other fluxes (J_{xfer}^{Mg}, J_{xfer}^{CaATP}, J_{xfer}^{MgATP}, J_{xfer}^{MgADP}) were added.

The calculations indicated that changes in free Ca^{2+} concentrations over the range of 0.13 to ~15 μM (9–10 s, metabolic inhibition) increased rest [CaATP]$_{ss}$/[MgATP]$_{ss}$ ratio ~11-fold and [CaATP]$_i$/[MgATP]$_i$ ratio ~2.3-fold. The fall in [ATP]$_{tot}$/[ADP]$_{tot}$ ratio did not have any significant effect on MgADP/MgATP ratios.

DISCUSSION

Model

The main goal of the present model was to study the role of ATP and ADP as Ca^{2+} and Mg^{2+} buffers, transporters, and ion-current regulators in the framework of the comprehensive ionic model of Winslow et al. (1999). Taking into consideration experimental and theoretical observations (Stern, 1992; Niggli and Lipp, 1993; Amstudz et al., 1996; Huser et al., 1996; Langer and Peskoff, 1996; Lipp and

Niggli, 1996; Soeller and Cannell, 1997; Jafri et al., 1998; Peskoff and Langer, 1998; Michailova et al., 1999; Niggli, 1999; Winslow et al., 1999; Huser et al., 2000) that Ca^{2+} near the plasma membrane can reach concentrations much higher than those in the bulk myoplasm, we allowed free and bound Mg^{2+}, ATP, and ADP concentrations near the membrane to differ from free and bound Mg^{2+}, ATP, and ADP concentrations in the bulk myoplasm.

Experimental and theoretical studies also indicate that ATP and ADP are mobile buffers (Zhou and Neher, 1993; Baylor and Hollingworth, 1998). To simulate diffusion of Mg^{2+}, ATP, and ADP from the subspace to the bulk myoplasm, we included fluxes for Mg^{2+}, CaATP, MgATP, CaADP, and MgADP.

In ventricular myocytes, low-affinity Ca^{2+} buffers ATP and ADP not only bind and transport Ca^{2+} and Mg^{2+} but also regulate intracellular enzymes, ATP-dependent transporters and channels (Kleber, 1983; Bers, 1991; Shaw and Rudy, 1997; Yokoshiki et al., 1998; Carmeliet, 1999). In muscle cells, MgATP is the preferred substrate for various ATPases (Bers, 1991; Kargacin and Kargacin, 1997; Carmeliet, 1999). From these experimental observations, we assumed that changes in diastolic and systolic [MgATP]$_i$ regulate SR Ca^{2+}-ATPase, Na$^+$-K$^+$ ATPase, and sarcolemmal Ca^{2+}-ATPase. In the model, pump currents and fluxes (J_{up}^{*}, I_{NaK}^{*}, $I_{p(Ca)}^{*}$) were proportional to [MgATP]$_i$.

Noma and Shibasaki (1985) reported the ATP-dependence of L-type Ca^{2+} current. Shaw and Rudy (1997) assumed direct ATP-dependence of I_{Ca} in their model. In our model, changes in total ATP and ADP concentrations indirectly regulate I_{Ca} via subspace Ca^{2+} concentration changes.

Here, it is important to emphasize that a major limitation of the Winslow et al. model (1999) is that, over a longer

time period, it fails to achieve a steady state. For $t > 15$ s: 1) $[Ca]_i$ and $[Ca]_{ss}$ peaks begin slowly to increase (for example, the $[Ca]_i$ peak increases to ~0.7 μM after 2 min periodic stimulation); 2) Systolic $[Na]_i$ and $[K]_i$ do not reach steady state even after 2 min; 3) Diastolic $[Na]_i$ increases to 14 mM, and diastolic $[K]_i$ decreases by 0.8 mM. In view of this, simulated Ca^{2+} transients in the original paper were computed at 9–10 s for comparison with experimentally measured steady-state responses in normal and failing canine ventricular myocytes. Similarly, in the present study, we examined the effects of ATP and ADP on the 10th cycles of stimulation (9–10 s).

Normal conditions

Our studies demonstrated that adding Ca^{2+} and Mg^{2+} exchange with stationary ATP (7 mM) and ADP (5 μM) did not significantly affect the high subspace Ca^{2+} signal, but was able to modify slightly the lower myoplasmic Ca^{2+} signal. Calculations showed that, under normal conditions, diffusion of ATP (as CaATP) might contribute to Ca^{2+} transport from subspace to myoplasm. Because $V_{myo} \gg V_{ss}$ ($V_{myo} = 25.84 \times 10^{-6}$ μL, $V_{ss} = 1.2 \times 10^{-9}$ μL), Ca^{2+} diffusion by the physiological concentration of the low-affinity Ca^{2+} buffer ATP (7 mM) was able to influence to some extent the Ca^{2+} signal in the subspace volume, but was unable to influence the Ca^{2+} signal in the myoplasmic volume. Our model predictions are in agreement with the conclusions of others (Kargacin and Kargacin 1997; Baylor and Hollingworth 1998) that Ca^{2+} binding by ATP and diffusion of Ca^{2+}-bound ATP may contribute to the determination of the amplitude and time course of intracellular Ca^{2+} signals. However, we need to emphasize that this common-pool model did not allow us to explore the effects of diffusion of CaATP on the local Ca^{2+} concentrations in the cell as predicted by Baylor and Hollingworth (1998).

The simulations also demonstrated that, under normal conditions, Ca^{2+} transport by ATP (as CaATP) increases the diastolic JSR Ca^{2+} level and systolic JSR Ca^{2+} peak slightly. Here it is important to note that a limitation of our model and of the model of Winslow et al. (1999) is that the SR is almost ⅔ depleted in a single beat. The experimental data of Janczewski et al. (1995) and Bassani et al. (1995) suggest a maximal SR depletion of no more than ~50%. Recently, Rice et al. (1999) extended the deterministic model of Jafri et al. (1998) by incorporating stochastic equations for the gain and gradedness of Ca^{2+} release in rat cardiac muscle. Simulations with the stochastic model showed that maximal SR depletion during a single beat is less than 50%.

Our results showed that the changes in $[Ca]_{ss}$ concentration after the inclusion of CaATP flux slightly affected the time course of I_{Ca}. Under normal conditions, the alterations in intracellular Ca^{2+}, Na^+, K^+, and MgATP concentrations and ion currents were small after the inclusion of ATP and ADP. Consequently, the simulated action potential was quite similar in shape to that shown by Winslow et al. (1999), (not shown in this article).

The model studies also suggest that, under normal conditions, changes in free Ca^{2+} concentrations during a single beat (9–10 s): 1) increased resting $[CaATP]_i$ whereas all other diastolic free and bound ATP and ADP concentrations remained almost unchanged; 2) were not able to affect the normal function of the ATP-regulated SR Ca^{2+} pump, Na^+-K^+, and sarcolemmal Ca^{2+} pump because S_{MgATP} (Eq. 25) remained fairly constant ~1; 3) significantly increased rest subspace and myoplasmic CaATP/MgATP ratios, while MgADP/MgATP concentration ratios were not affected.

Metabolic inhibition

The major pathophysiological effects of ischemia include the accumulation of $[K]_0$, acidosis (intra- and extracellular pH drop) and anoxia (fall in $[ATP]_{tot}/[ADP]_{tot}$ ratio and opening of the specific ATP-sensitive K^+ channels), (Shaw and Rudy, 1997; Carmeliet, 1999). The present model provided an opportunity to investigate how the fall in $[ATP]_{tot}/[ADP]_{tot}$ ratio could affect intracellular ion concentrations, free and bound ATP and ADP concentrations, and ionic currents. In this study, the extracellular K^+ was constant at normal value (4 mM) throughout the simulations with $[ATP]_{tot}/[ADP]_{tot}$ unity or ATP and ADP 0 mM.

The most important result was the observation that changes in the diastolic $[MgATP]_i$, as consequence of the changes in $[ATP]_{tot}/[ADP]_{tot}$ ratio, significantly affected ATPase pump activities, in turn altering normal ion and buffer concentrations and ion currents. The model predicted that: 1) during metabolic inhibition ($[ATP]_{tot}/[ADP]_{tot} = 1$), diastolic $[MgATP]_i$ decreases ~50% and remains fairly constant in the face of $[Ca]_i$ concentration changes from 0.13 to 0.37 μM (9–10 s); and 2) with total metabolic inhibition ($[ATP]_{tot} = [ADP]_{tot} = 0$ mM) the diastolic $[MgATP]_i$ is zero.

The model studies demonstrated that, when $[ATP]_{tot}$ and $[ADP]_{tot}$ were 3 mM: 1) normal SR Ca^{2+} content significantly decreases; 2) normal diastolic $[Ca]_{ss}$ increases, $[Ca]_{ss}$ peak drops ~50%, $[Ca]_{ss}$ decay rate increases, and pathological $[Ca]_{ss}$ transient reaches rest level earlier than normal; and 3) normal diastolic $[Ca]_i$ increases, the earlier $[Ca]_i$ peak drops ~50% and a second, higher and slower, $[Ca]_i$ peak emerges. The simulations also show that the decline in the earlier $[Ca]_i$ peak coincides with depletion of the JSR. The appearance of a second higher $[Ca]_i$ peak under ischemic conditions can be attributed to the increased Ca^{2+} influx through L-type Ca^{2+} channels. In addition, the model predicts the appearance of a second slow peak in the free $[ATP]_i$ transient, in the free $[Mg]_i$ transient, and in all other free and bound ATP and ADP transients. The simulation results also indicate that, under total metabolic inhibition ($[ATP]_{tot} = 0$ mM, $[ADP]_{tot} = 0$ mM), the SR is almost

empty, diastolic Ca^{2+} levels increase further, systolic Ca^{2+} levels decrease, and the earlier $[Ca]_i$ peak disappears. With total ATP and ADP inhibition, the SR and sarcolemmal Ca^{2+} ATPase were fully down-regulated and Na^+/Ca^{2+} exchanger efficiency decreased further. Our analysis suggests that the most important reasons for these changes in normal $[Ca]_{JSR}$, $[Ca]_{ss}$, and $[Ca]_i$ transients were reduced Ca^{2+} uptake by SERCA2a pump and reduced Ca^{2+} release from JSR. In the Winslow et al. (1999) model, where ATP and ADP were not included, the effect of down-regulation of SERCA2a pump during heart failure was simulated by varying a scaling factor for Ca^{2+} ATPase (K_{SR}) from 1.0 to 0.0. Our model predictions for the reduced SR Ca^{2+} content, increased diastolic Ca^{2+} and decreased systolic Ca^{2+} during ischemia are in agreement with experimental observations (Griese, 1988; Isenberg et al., 1993; Martin et al., 1998; Carmeliet, 1999). Measuring free $[Ca]_i$ concentrations by indo 1 fluorescence in a voltage-clamped myocyte, Isenberg and co-workers (1993) also observed that a fall in systolic $[Ca]_i$ during metabolic inhibition ($[ATP]_{tot} = [ADP]_{tot} = 3$ mM) or during total metabolic inhibition ($[ATP]_{tot} = [ADP]_{tot} = 0$ mM) may be accompanied by oscillations. This model failed to simulate the systolic $[Ca]_i$ oscillations. Our studies showed that the earlier $[Ca]_i$ peak disappears when Ca^{2+} uptake by SERCA2a pump is totally blocked (Fig. 5 *B*, solid and dash-dot lines). The earlier $[Ca]_i$ peak (knob) is an artifact of the common-pool model assumptions and depends on SR Ca^{2+} release (Winslow et al., 1999). Additionally, we conclude that the earlier peaks in the free $[ATP]_i$ transient, in the free $[Mg]_i$ transient and in all other free and bound ATP and ADP transients are also common-pool model artifacts. Recently, developing a local control model of Ca^{2+} release in the cardiac diadic space, Rice et al. (1999) found that the simulated $[Ca]_i$ transient increases gradually and did not exhibit the knob.

Experimental studies in guinea pig hearts suggest that ~3 mM ATP and elevated extracellular K^+ concentration (~12 mM) are able to support Na^+-K^+ pump function, i.e., that significant changes in normal I_{NaK} do not occur during acute ischemia (Kleber, 1983). For this reason, equations describing the ATP-dependence of the Na^+-K^+ pump were not included in the Shaw and Rudy model (1997). Because it is well established (Bers, 1991; Fozzard and Lipkind, 1995; Carmeliet, 1999) that Na^+-K^+ pump function is strongly ATP-dependent (for each ATP molecule consumed three Na^+ and two K^+ are transported), we included equations describing the ATP-dependence of Na^+-K^+ ATPase. Our simulations predicted that the Na^+-K^+ ATPase activity is reduced with $[ATP]_{tot}$ and $[ADP]_{tot}$ 3 mM and extracellular K^+ normal (see Fig. 6 *C*, solid line). Additionally, 3 mM ATP and 12 mM $[K]_0$ (not shown) were also not able to support normal Na^+-K^+ pump function (rest I_{NaK} increased from 0.025 to 0.06 pA/pF and from 0.05 to 0.128 pA/pF during excitation). Na^+-K^+ pump function is sensitive to $[Na]_i$ and $[Na]_0$ concentration changes. It is possible that the

predicted pathological I_{NaK} were not in agreement with the observations of Kleber (1983) because diastolic and systolic $[Na]_i$ were not correctly simulated, and because $[Na]_0$ was constant during periodic stimulation. Another reason could be that I_{NaK} may not be proportional to $[MgATP]_i$ as assumed in Eq. 22. Nevertheless, making the same approximation for currents carried by the sarcolemmal Ca^{2+}-ATPase and SR Ca^{2+}-ATPase transporters resulted in good qualitative agreement with experimental observations of Ca^{2+} signals under normal and pathological conditions (Griese, 1988; Bers, 1991; Isenberg et al., 1993; Martin et al., 1998; Carmeliet, 1999).

In contrast to the significant changes in I_{Ca}, I_{NaCa}, I^*_{NaK}, and $I^*_{p(Ca)}$, the predicted effects of metabolic inhibition on $I_{Ca,K}$, $I_{Ca,b}$, I_{Na}, I_{K1}, and $I_{Na,b}$ currents were negligible. It is interesting that our model, where ATP regulates indirectly I_{Ca} via $[Ca]_{ss}$, like that of Shaw and Rudy (1997), where ATP regulates I_{Ca} directly, also predicts an increase in Ca^{2+} influx through L-type channels after a fall in total ATP concentration. The normal time courses of I_{Kr}, I_{Ks}, I_{to1}, and I_{Kp} remain unchanged after 10 s stimulation.

Action potential duration in the model increased after a fall in $[ATP]_{tot}$ with 4 mM extracellular K^+. The analysis suggests that only the down-regulation of the SR Ca^{2+}-ATPase significantly influenced action potential shape, whereas the effect of Na^+-K^+ or sarcolemmal ATPase down-regulation was negligible. Winslow et al. (1998), varying the scaling factor for SR Ca^{2+}-ATPase from 1.0 to 0.0, also observed an increase in action potential duration. Our results demonstrated that diastolic $[MgATP]_i$ (or S_{MgATP}) remains fairly constant during a single beat (9–10 s). Under normal conditions, S_{MgATP} was unity, for metabolic inhibition, S_{MgATP} was ~0.488, and for total metabolic inhibition, S_{MgATP} was zero. Because the simulated action potential is similar to that shown in the original paper, it is not shown again here. In contrast with these predictions, experimental and theoretical studies (Gettes and Cascio, 1992; Cascio et al., 1995; Shaw and Rudy, 1997; Carmeliet, 1999) show a well-known shortening of action potential duration during ischemia (note here $[K]_0 = 12$ mM, pH = 6.5, $[ATP]_{tot} = 3$ mM, ATP-sensitive K^+ channels open).

Experimental data suggest that, under metabolic inhibition, free intracellular Mg^{2+} concentration may increase to 2–6 mM (Kirkels et al., 1989; Murphy et al., 1989; Carmeliet, 1999). In our simulations, diastolic Mg^{2+} increased from 1 to ~2.25 mM when $[ATP]_{tot}/[ADP]_{tot}$ was unity and to 7.44 mM when ATP and ADP were zero. The calculations also showed that when $[ATP]_{tot}$ and $[ADP]_{tot}$ are 3 mM and Mg^{2+} is 2.25 mM: 1) diastolic ATP, CaATP, and MgATP concentrations decrease ~80%, ~70%, and ~50%, whereas diastolic ADP, CaADP, and MgADP concentrations increase ~345-, ~500-, and ~767-fold; 2) systolic $[CaADP]_{ss}$ and $[CaATP]_{ss}$ increase more notably from initial diastolic levels than all other systolic free and bound

ATP and ADP concentrations. An interesting model prediction was that, during metabolic inhibition, the diffusion of Ca^{2+}-bound ADP contributes to Ca^{2+} transport from the subspace to myoplasm, while the importance of CaATP flux decreases. During metabolic inhibition, changes in intracellular Ca^{2+} had a considerable effect on CaATP/MgATP ratios in the subspace and myoplasm but no effect on MgADP/MgATP ratios.

The model also predicted that, in ventricular myocytes, high Ca^{2+} concentrations near the membrane could stimulate greater changes in free and bound Mg^{2+}, ATP, and ADP concentrations than could be elicited by the lower Ca^{2+} signal in the myoplasm.

Incorporating equations for Ca^{2+} and Mg^{2+} buffering and transport by ATP and ADP and equations for ATP regulation of ion transporters in the model of Winslow et al. (1999), we developed a more detailed biophysical and biochemical model that connected Ca^{2+} signaling and cell electrophysiology with cell metabolism. This model was able to reproduce qualitatively a sequence of events that corresponds well with experimental data in normal and pathological conditions (Marban et al., 1990; Wagner et al., 1990; Isenberg et al., 1993; Wilde and Aksnes, 1995; Carmeliet, 1999). It needs to be refined however, because many of the important processes occurring during ischemia and reperfusion were not included: 1) metabolism of high-energy phosphates, ATP-sensitive K^+ channels, Na^+-activated K^+ current, counterion anion channels in the SR, glycogen metabolism, and lactate transport regulation (Ch'en et al., 1998; Noma, 1983; Shaw and Rudy, 1997; Eager and Dulhunty, 1998; Faber and Rudy, 2000); 2) changes in extracellular K^+, Na^+, and Ca^{2+} concentrations during metabolic inhibition (Wilde and Aksnes, 1995; Shaw and Rudy, 1997; Carmeliet, 1999); 3) decreased extracellular and intracellular pH during metabolic inhibition (Kleber, 1983; Orchard and Kentish, 1990; Shaw and Rudy, 1997; Ch'en et al., 1998); 4) binding of Mg^{2+} to troponin C and calmodulin, that additionally may affect free intracellular Mg^{2+} and Ca^{2+} concentrations (Robertson et al., 1981); 5) cell volume changes (Wright and Rees, 1997; Carmeliet, 1999); 6) changes in fatty acids (Corr et al., 1995); and 7) production of free radicals (Manning and Hearse, 1984; Carmeliet, 1999).

REFERENCES

Amstudz, C., A. Michailova, and E. Niggli. 1996. The role of local events and diffusion in cardiac EC-coupling. *Biophys. J.* 70:A274. (Abstr.)

Bassani, J. W., W. Yuan, and D. M. Bers. 1995. Functional SR Ca release is regulated by trigger Ca and SR content in cardiac myocytes. *Am. J. Physiol. Cell Physiol.* 268:C1313–C1329.

Baylor, S. M., and S. Hollingworth. 1998. Model of sarcomeric Ca^{2+} movements, including ATP Ca^{2+} binding and diffusion, during activation of frog skeletal muscle. *J. Gen. Physiol.* 112:297–316.

Bers, D. M. 1991. Excitation-Contraction Coupling and Cardiac Contractile Force. Kluwer, Boston. 46–47.

Carmeliet, E. 1999. Cardiac ionic currents and acute ischemia: from channels to arrhythmias. *Physiol. Rev.* 79:917–1017.

Cascio, W. E., T. A. Johnson, and L. S. Gettets. 1995. Electrophysiologic changes in ischemic ventricular myocardium: I. Influence of ionic, metabolic and energetic changes. *J. Cardiovasc. Electrophys.* 6:1039–1062.

Ch'en, F., K. Clarke, R. Vaughan-Jones, and D. Noble. 1997. Modeling of internal pH, ion concentration, and bioenergetic changes during myocardial ischemia. *Adv. Exp. Med. Biol.* 430:281–290.

Ch'en, F. F. T., R. D. Vaughan-Jones, K. Clarke, and D. Noble. 1998. Modelling myocardial ischemia and reperfusion. *Prog. Biophys. Mol. Biol.* 69:515–538.

Corr, P. B., K. A. Yamada, M. H. Creer, J. Wu, J. McHowat, and G. X. Yan. 1995. Amphipathic lipid metabolites and arrhythmias during ischaemia. *In* Cardiac Electrophysiology: From Cell to Bedside. D. P. Zipes and J. Jalife, editors. W.B. Saunders, Philadelphia. 182–203.

Dawson, S. P., J. Keizer, and J. E. Pearson. 1999. Fire-diffuse-fire model of dynamics of intracellular calcium waves. *Proc. Nat. Acad. Sci. U.S.A.* 96:6060–6063.

Eager, K. R., and A. F. Dulhunty. 1998. Activation of the cardiac ryanodine receptor by sulfhydryl oxidation is modified by Mg^{2+} and ATP. *J. Membrane Biol.* 163:9–18.

Faber, G. M., and Y. Rudy. 2000. Action potential and contractility changes in $[Na]_I$ overload cardiac myocytes: a simulation study. *Biophys. J.* 78:2392–2404.

Fozzard, H. A., and G. Lipkind. 1995. Ion channels and pumps in cardiac function. *Adv. Exp. Med. Biol.* 382:3–10.

Gettets, L. S., and W. E. Cascio. 1992. Effect of acute ischemia on cardiac electrophysiology. *In* The Heart and Cardiovascular System. H. A. Fozzard, R. B. Jennings, E. Haber, A. M. Katz and H. E. Morgan, editors. Raven Press, New York. 2021–2054.

Griese, M., V. Perlitz, E. Jungling, and H. Kammermeier. 1988. Myocardial performance and free energy of ATP-hydrolysis in isolated rat hearts during graded hypoxia, reoxygenation and high K_e^+ perfusion. *J. Mol. Cell Cariol.* 20:1189–1201.

Hunter, P. J., A. D. McCulloch, and H. E. D. J. ter Keurs. 1998. Modelling the mechanical properties of cardiac muscle. *Prog. Biophys. Mol. Biol.* 69:289–331.

Huser, J., S. L. Lipsius, and L. A. Blatter. 1996. Calcium gradients during excitation–contraction coupling in cat atrial myocytes. *J. Physiol.* 494:641–651.

Huser, J., Y. G. Wang, K. A. Sheehan, F. Cifuentes, S. L. Lipsius, and L. A. Blatter. 2000. Functional coupling between glycolysis and excitation–contraction coupling underlies alternans in cat heart cells. *J. Physiol.* 524:795–806.

Imredy, J. P., and D. T. Yue. 1994. Mechanism of Ca^{2+}-sensitive inactivation of L-type Ca^{2+} channels. *Neuron.* 12:1301–1318.

Isenberg, G., S. Han, A. Schiefer, and M. F. Wendt-Gallitelli. 1993. Changes in mitochondrial calcium concentration during the cardiac contraction cycle. *Cardiovasc. Res.* 27:1800–1809.

Jafri, M. S., J. J. Rice, and R. L. Winslow. 1998. Cardiac Ca^{2+} dynamics: the roles of ryanodine receptor adaptation and sarcoplasmic reticulum load. *Biophys. J.* 74:1149–1168.

Janczewski, A. M., H. A. Spurgeon, M. D. Stern, and E. D. Lakatta. 1995. Effects of sarcoplasmic Ca^{2+} load on the gain function of Ca^{2+} by Ca^{2+} current in cardiac cells. *Am. J. Physiol. Heart Circ. Physiol.* 268:H916–H920.

Kargacin, M. E., and G. J. Kargacin. 1997. Predicted changes in concentrations of free and bound ATP and ADP during intracellular Ca^{2+} signaling. *Am. J. Physiol. Cell Physiol.* 273:C1416–C1426.

Keizer, J., and L. Levine. 1996. Ryanodine receptor adaptation and Ca^{2+}-induced Ca^{2+} release-dependent Ca^{2+} oscillations. *Biophys. J.* 71:3477–3487.

Kirkels, J. H., C. J. van Echteld, and T. J. Ruigrok. 1989. Intracellular magnesium during myocardial ischemia and reperfusion: possible consequences for postischemic recovery. *J. Mol. Cell. Cardiol.* 21:1209–1218.

Kleber, A. G. 1983. Resting membrane potential, extracellular potassium activity, and intracellular sodium activity during acute global ischemia in isolated perfused guinea pig hearts. *Circ. Res.* 52:442–450.

Langer, G. A., and A. Peskoff. 1996. Calcium concentration and movement in the diadic cleft space of the cardiac ventricular cell. *Biophys. J.* 70:1169–1182.

Leyssens, A., A. V. Nowicky, L. Patterson, M. Crompton, and M. R. Duchen. 1996. The relationship between mitochondrial state, ATP hydrolysis, [Mg^{2+}]$_i$ and [Ca^{2+}]$_i$ studied in isolated rat cardiomyocytes. *J. Physiol.* 496:111–128.

Lipp, P., and E. Niggli. 1996. Submicroscopic calcium signals as fundamental events of excitation–contraction coupling in guinea-pig cardiac myocytes. *J. Physiol.* 492:31–38.

Luo, C. H., and Y. Rudy. 1994. A dynamic model of the cardiac ventricular action potential. I. Simulations of ionic currents and concentration changes. *Circ. Res.* 74:1071–1096.

Manning, A. S., and D. J. Hearse. 1984. Reperfusion-induced arrhythmias: mechanisms and prevention. *J. Mol. Cell. Cardiol.* 16:497–518.

Marban, E., M. Kitakaze, Y. Koretsune, D. T. Yue, V. P. Chacko, and M. M. Pike. 1990. Quantification of [Ca^{2+}]$_i$ in perfused hearts. Critical evaluation of the ^{5}F-BAPTA and nuclear magnetic resonance method as applied to study of ischemia and reperfusion. *Circ. Res.* 66:1255–1267.

Martell, A. E., and R. M. Smith. 1982. Critical Stability Constants, Vol. 5, 1st Suppl. Plenum Press, New York.

Martin, B. J., H. Valdivia, R. Bunger, R. D. Lasley, and R. M. Mentzer. 1998. Pyruvate augments calcium transients and cell shortening in rat ventricular myocytes. *Am. J. Physiol. Heart Circ. Physiol.* 274:H8–H17.

Michailova, A., and V. Spassov. 1992. Theoretical model and computer simulation of excitation–contraction coupling of mammalian cardiac muscle. *J. Mol. Cell. Cardiol.* 24:97–104.

Michailova, A., F. DelPrincipe, D. Duridanova, and E. Niggli. 1999. Computer modeling of Ca^{2+} diffusion during Ca^{2+} signaling in atrial cells. *Biophys. J.* 76:A459. (Abstr.)

Murphy, E., C. Steenbergen, L. A. Levy, B. Raju, and R. E. London. 1989. Cytosolic free magnesium levels in ischemic rat heart. *J. Biol. Chem.* 264:5622–5627.

Negroni, J. A., and E. C. Lascano. 1996. A cardiac muscle model relating sarcomere dynamics to calcium kinetics. *J. Mol. Cell. Cardiol.* 28:915–929.

Niggli, E., and P. Lipp. 1993. Subcellular restricted spaces—significance for cell signalling and excitation-contraction coupling. *J. Muscle Res. Cell. Motil.* 14:288–291.

Niggli, E. 1999. Localized intracellular calcium signaling in muscle: calcium sparks and calcium quarks. *Annu. Rev. Physiol.* 61:311–335.

Noma, A. 1983. ATP regulated K$^+$ channels in cardiac muscle. *Nature.* 305:147–148.

Noma, A., and T. Shibasaki. 1985. Membrane current through adenosine-triphosphate-regulated potassium channels in guinea-pig ventricular cells. *J. Physiol. (Lond.).* 363:463–480.

Nygren, A., C. Fiest, L. Firec, J. W. Clark, D. S. Lindblad, R. B. Clark, and W. R. Giles. 1998. Mathematical model of an adult human atrial cell. The role of K$^+$ currents in repolarization. *Circ. Res.* 82:63–81.

Orchard, C. H., and J. C. Kentish. 1990. Effects of changes of pH on the contractile function of cardiac muscle. *Am. J. Physiol. Cell Physiol.* 258:C967–C981.

O'Rourke, B., D. A. Kass, G. F. Tomaselli, S. Kaab, R. Tunin, and E. Marban. 1999. Mechanisms of altered excitation–contraction coupling in canine tachycardia-induced heart failure. I: Experimental studies. *Circ. Res.* 84:562–570.

Peskoff, A., and G. A. Langer. 1998. Calcium concentration and movement in the ventricular cardiac cell during an excitation–contraction coupling cycle. *Biophys. J.* 74:153–174.

Ralston, A., and H. S. Wilf. 1960. Mathematical Method for Digital Computers. Wiley, New York.

Rice, J., S. Jafri, and R. Winslow. 1999. Modeling gain and gradedness of Ca^{2+} release in the functional unit of the cardiac diadic space. *Biophys. J.* 77:1871–1884.

Robertson, S. P., J. D. Johnson, and J. D. Potter. 1981. The time course of Ca^{2+} exchange with calmodulin, troponin, parvalbumin, and myosin in response to transient increase in Ca^{2+}. *Biophys. J.* 34:559–569.

Shaw, R. M., and Y. Rudy. 1997. Electrophysiologic effects of acute myocardial ischaemia: a theoretical study of altered cell excitability and action potential duration. *Cardiovasc. Res.* 35:256–272.

Soeller, C., and M. B. Cannell. 1997. Numerical simulation of local calcium movements during L-type calcium channel gating in the cardiac diad. *Biophys. J.* 73:97–111.

Stern, M. 1992. Theory of excitation–contraction coupling in cardiac muscle. *Biophys. J.* 63:497–517.

Wagner, S., S. T. Wu, W. W. Parmley, and J. W. Coffelt. 1990. Influence of ischemia on [Ca^{2+}]$_i$ transients following drug therapy in hearts from aortic constructed rats. *Cell Calcium.* 11:431–444.

Wilde, A. A., and G. Aksnes. 1995. Myocardial potassium loss and cell depolarization in ischaemia and hypoxia. *Cardiovasc. Res.* 29:1–15.

Winslow, R. L., J. Rice, and S. Jafri. 1998. Modeling the cellular basis of altered excitation–contraction coupling in heart failure. *Prog. Biophys. Mol. Biol.* 69:497–514.

Winslow, R. L., J. Rice, S. Jafri, E. Marban, and B. O'Rourke. 1999. Mechanisms of altered excitation–contraction coupling in canine tachycardia-induced heart failure. II. Model studies. *Circ. Res.* 84:571–586.

Wright, A. R., and S. A. Rees. 1997. Targeting ischaemia: cell swelling and drug efficacy. *TiPS* 18:224–228.

Yokoshiki, H., M. Sunagawa, T. Seki, and N. Sperelakis. 1998. ATP-sensitive K$^+$ channels in pancreatic, cardiac, and vascular smooth muscle cells. *Am. J. Physiol. Cell Physiol.* 274:C25–C37.

Zhou, Z., and E. Neher. 1993. Mobile and immobile calcium buffers in bovine adrenal chromaffin cells. *J. Physiol. (Lond.).* 469:245–273.

Zoghbi, M. E., P. Bolanos, C. Villalda-Galea, A. Marcano, E. Hernandez, M. Fill, and A. L. Escobar. 2000. Spatial Ca^{2+} distribution in contracting skeletal and cardiac muscle cells. *Biophys. J.* 78:164–173.